This chapter is mainly focused on modified adsorbent of Sn-ATMP through sol-gel process. Sn-ATMP is characterized using ICP, CHN, FTIR, XRD, SEM-EDX and TGA. The cationic dye adsorption study (i.e, MB, MG, CV, RHB) of the prepared adsorbent is also discussed. Waste water treatment can benefit from the use of the modified Sn-ATMP.

6.1. Introduction

Fears regarding water pollution have become prevalent in the scientific community as a whole in recent decades [1]. In comparison to the entire volume of water on Earth, freshwater resources are limited. Dye is one of the main types of water pollution caused by industrial activity [2,3]. The textile industry is among the more regulated and fastest growing industrial sectors. There are numerous dyes available, including cationic, anionic and non-ionic types. Due to their solubility in water, chemical stability and difficulty in naturally biodegrading within the environment, cationic dyes are mainly employed in the textile and painting industries for colouring [4]. Dyes are potentially harmful aromatic compounds with intricate aromatic structures. Methylene blue (MB), malachite green (MG), crystal violet (CV), and rhodamine B (RHB) are a few of the most often employed cationic dyes. These dyes find application in the industrial sectors [5-7]. The longevity of MB, MG, CV, and RHB dyes in wastewater from factories poses a threat to human and aquatic health [8]. In this respect, it is critical to find an environmentally sound way to eradicate dye from wastewater and repurpose the dye and water. Nowadays, dyes are being utilized for removing of wastewater from industries using an assortment of techniques [9-14]. The composition of the wastewater, operating expenses, style of dye, and waste products emitted are factors that impact each technique's technical and financial viability. Soluble dyes are not well-suited for the coagulation process, which decolorizes insoluble dyes efficiently. Large amounts of sludge buildup are also seen. Nearly all dyes, with the exception of dispersion dyes, become decolorized through oxidation processes like ozonation; nevertheless, chemical oxygen demand COD is not effectively eliminated. Trade dyes are not successfully decoloured by the biological process. As a result, achieving total decolorization necessitates the implementation of multiple techniques. Consequently, a variety of approaches are used to create dye-removal procedures [15].

In the sorption processes of adsorption and ion exchange, specific adsorptive materials are specifically moved from the fluid phase to the surface of insoluble, inflexible particles that are either packed in a column or suspended in a reservoir. Due to its straightforward design, low initial cost, convenience of use, and insensitivity to harmful pollutants, adsorption has been

a popular technique for removing dissolved contaminated organic molecules [16]. Ion exchange phenomena is usually employed in the industrial sector to demineralize and soften water, among other purposes. This technique also eliminates ionic and water-soluble organic debris. This approach is also highly effective for eradicating dissolved contaminants such as colorants [17]. Many appropriate sorbents have been utilized, including polymeric resins [18], activated carbon [19], clay minerals [20], zeolites [21] and an assortment of inexpensive adsorbents [22].

Nowadays, there's a lot of curiosity in designing mixed materials, or organic/inorganic composites, where the qualities of the inorganic and organic constituents work well together to create new materials with unique composite properties and solid-state structures [23] which is known as tetravalent metal acid (TMA) salts. To deal with the phosphonic acids that arise, tetravalent metals like Zr, Ti, Sn, Th, Ce, and so forth can be employed to create new metal phosphonates by replacing R (where R = alkyl or aryl) for H or OH in the tetrahedral component of phosphoric acid, $PO(OH)_3$ [24–26]. The emphasis continues to be on clarifying the structure, despite the conjunction and characterization of many metal phosphonates. These materials' potential use in materials chemistry, as sorbents, and as ion exchangers rendering them intriguing [27]. The following functional groups (-OH, -COOH, $-SO_3H$, NO_2, N=N, etc.) are generally present in dye structures in a few of these forms. It is thought that during adsorption, the functional groups specified above can engage via covalent, coulombic, hydrogen bonding, or weak Van der Waals forces with the matrix material or sorbent being employed. The kind and intensity of the dye-sorbent interaction influences how well the dye can be rinsed out. Ion exchange materials (metal phosphonate) have been employed as sorbents to remove colored wastewaters have been described in the literature [28], calcium aminodiphosphonates (CadP) [29], Periodic mesoporous titanium phosphonates (PMTP-1) [30] and some other phosphonates [31-34].

In this instance, tetravalent tin chloride (as $SnCl_4 \cdot 5H_2O$) and amino tris-(methylene phosphonic acid) (ATMP) are used to synthesis a novel metal phosphonate, abbreviated as (Sn-ATMP), a hybrid ion exchange material belonging to the tetravalent metal acid (TMA) salt class. The sol-gel method was used in this endeavour. The substance has undergone (ICP-AES), CHN, FTIR, SEM-EDS, TGA and X-ray diffraction assessments. Evaluation of the material's chemical resistivity in a variety of environments. Structural hydroxyl groups are present in metal phosphonate (Sn-ATMP), with the hydroxyl groups' H determining the cation exchange

behaviour. Owing of the hydroxyl groups in structure, it is anticipated that the dye will either form weak Van der Waals forces or hydrogen bonds with the matrix material (Sn-ATMP), facilitating sorption and desorption. Therefore, it was deemed to be interesting to treat wastewater containing colours by using metal phosphonate as a sorbent. Sn-ATMP's ability to adsorb the target pollutant, the cationic dye (MB, MG, CV, RHB), from aqueous solution have been assessed batch study. The specifics of the cationic dye adsorption onto SNATMP's kinetics, thermodynamics, and adsorption isotherms are discussed. The desorption method was used to conduct the regeneration investigation of the Sn-ATMP sorbent.

6.2. Experimental section

6.2.1. Materials, methods and characterization

"Chapter 2" (Sections 2.1, 2.2, 2.3 and 2.4) provides an exhaustive description of all the chemical materials, techniques, and physical measurements utilized in the present work.

6.2.2. Adsorption study

A stock solution of MB, MG, CV and RHB (1000 mg/L) dyes were prepared by dissolving appropriate amount of each dye in deionized water. The adsorption experiments have been carried out in conical flask with aluminium foil closures on a rotary shaker with a constant 120 rpm agitation speed. Different aspects of the experiment were investigated with each dye solution (25 mL), including analyte pH (2-11), dose (10-200 mg), concentration (30-500 mg/L), contact time (5-120 min) and temperature (25-55°C) that can influence the he materials' adsorption efficiency. Dilute solutions of HCl and NaOH were used to modify the pH of the solutions under evaluation. The temperature was controlled with using a thermostatically controlled incubator.

The dye concentration within the solution after and before adsorption experiment might be examined by inspecting characteristic absorbance of these dyes in ultraviolet-visible (UV-Vis) spectra, i.e. λ_{max} = 664 nm for MB, λ_{max} = 617 nm for MG, λ_{max} = 590 nm for CV and λ_{max} = 556 nm for RHB. To do this, adsorption-concentration calibration curve had been first established for each dye separately, using the standard solutions. Then, the calibration curves were employed to determine the unknown concentration **(Figure 6.1)**. It is fitted using a linear fit. The adsorption capacity at equilibrium (q_e) and the efficiency of removal in percentage (R%) of each dye have been estimated by the equations as previously mentioned in "Chapter 4" (Sec 4.2.4).

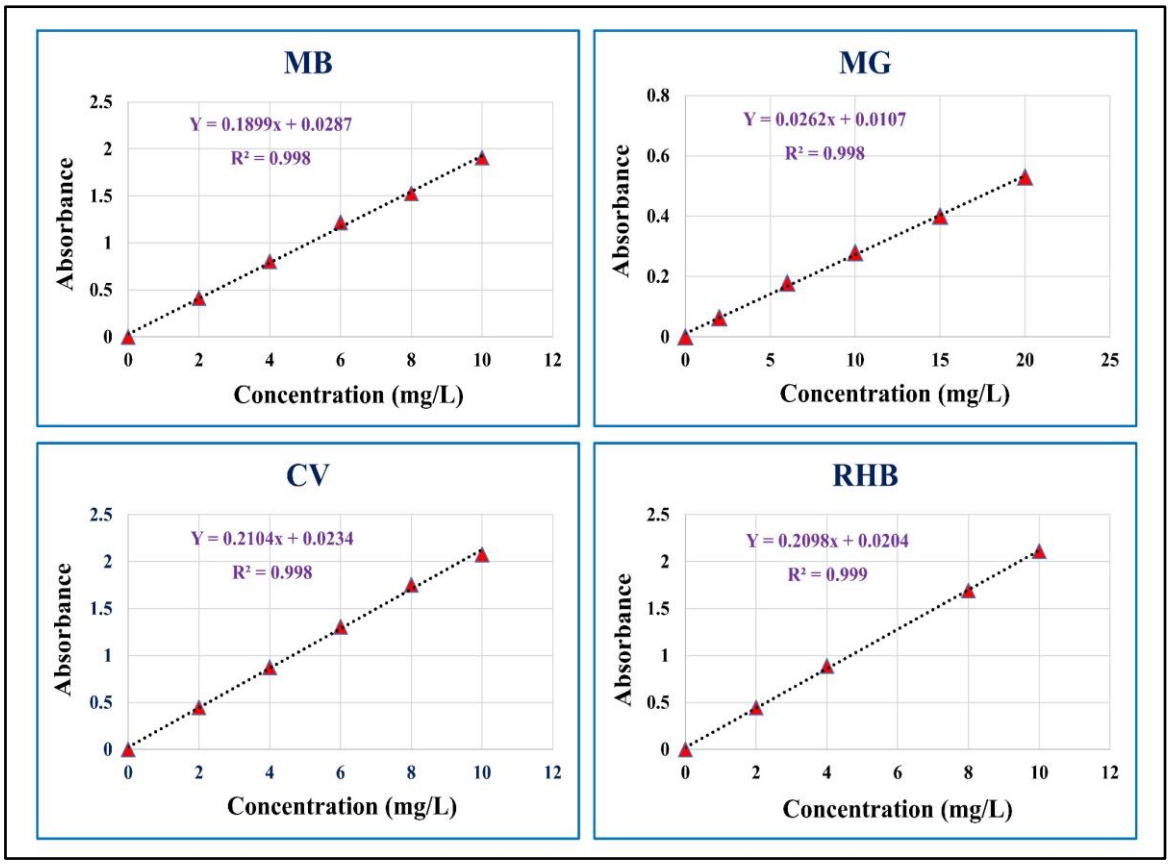

Figure 6.1. Calibration curve of MB, MG, CV and RHB using standard solution.

6.2.3. Adsorption kinetics

Time-dependent process of adsorption and the involved mechanism of the adsorption kinetics data for MB, MG, CV, RHB were investigated by applying three adsorption kinetics models, namely the pseudo-first-order and pseudo-second-order and the intraparticle diffusion model as previously stated in "Chapter 3" (Sec. 3.2.4, 3.2.4.1, 3.2.4.2, 3.2.4.3).

6.2.4. Isotherms of adsorption

Studies of equilibrium offer useful insights into the adsorption dynamics. Especially when the adsorption process approaches an equilibrium state, equilibrium studies help to clarify the essence of the connection between adsorbed material and adsorbent. In current work, the data at equilibrium were examined using the Freundlich and Langmuir isotherm models. The mathematical Freundlich and Langmuir adsorption isotherms linear equations followed the prior "Chapter 4" (Sec. 4.2.3.1) exposition.

6.2.5. Thermodynamics parameters

Thermodynamics parameters follow the previous "Chapter 4" (Sec.4.2.3.3) description.

6.2.6. Desorption/Reusability Study

Solution (50 mg/L) of MB, MG, CV and RHB was loaded on Sn-ATMP (80 mg) with constant shaking at natural pH and 298 K. Shaking time for MB and MG was 50 minutes and for CV and RHB was 60 minutes with Sn-ATMP. In order to assess the dye adsorption at the surface of Sn-ATMP, the residual concentration of MB, MG, CV and RHB in the solution was evaluated. After that, MB@Sn-ATMP, MG@Sn-ATMP, CV@Sn-ATMP and RHB@Sn-ATMP intricate was dried at 60°C for a period of 24 hours. Subsequently, 10 mL of 0.05 M HCl for MB and RHB and 0.1 M EDTA for MG and CV was added into conical flasks at natural pH. Flasks have shaked with 120 rpm for 1 hrs. The amount of desorbed dye was measured at a particular wavelength by using an UV-vis spectrophotometer.

6.3. Results and discussion

6.3.1. Physico-chemical and ion exchange characteristics of Sn-ATMP

In the current investigation, Sn (IV) phosphonate, a novel organic-inorganic ion exchanger containing a high capacity for ion exchange, was created as an adsorbent. An opaque, firm, white granule was observed to represent Sn-ATMP. **Table 6.1** displays Sn-ATMP's physical and ion-exchange characteristics. pH titration curve as weak cation exchanger shown in **Figure 6.2.** Equipped with 190 ml of 0.5 M sodium acetate solution, the Na^+ ion exchange capacity (CEC) in meq.g^{-1} derived by the column technique at room temperature is 3.84 meq·g^{-1}, as seen in **Figures 6.3 (a) and (b)**. According to a study, Sn-ATMP exhibits chemical stability in both acidic and organic solvent circumstances. However, in base medium, it is not as stable. **Table 6.1** presents the maximum allowable limits. The impact of calcination on the CEC was utilized to further explore the material's thermal behavior. The sample's CEC after being calcined at intervals of 50 °C from 50 to 400 °C.

Table 6.1. Physico-chemical and ion exchange characteristics of Sn-ATMP.

Physicochemical Characteristics of Sn-ATMP			
Materials			Sn-ATMP
Appearance			White opaque granules
Moisture content			7.33%
Particle size (range)			0.23-0.51 mm
Apparent density			0.52 $g.mL^{-1}$
True density			1.77 $g.mL^{-1}$
Chemical stability (Maximum tolerable limits)	Acid	H_2SO_4	3N
		HNO_3	5N
		HCL	5N
	Base	NaOH	0.5N
		KOH	0.5N
	Organic solvents	Ethanol, acetone, acetic acid	Stable

Ion Exchange Characteristics of Sn-ATMP		
Materials		Sn-ATMP
Void volume fraction		0.70
Concentration of fixed ionogenic group		6.29 $mmol \cdot g^{-1}$
Volume capacity		1.88 $meq.mL^{-1}$
Nature of exchanger based on pH titration curve		Weak Cation Exchanger
Ion exchange capacity (IEC) ($meq.g^{-1}$)	~30 °C (RT)	3.84
	50 °C	3.44
	100 °C	3.05
	150 °C	2.88
	200 °C	2.45
	250 °C	2.10
	300 °C	1.95
	350 °C	1.90
	400 °C	1.70

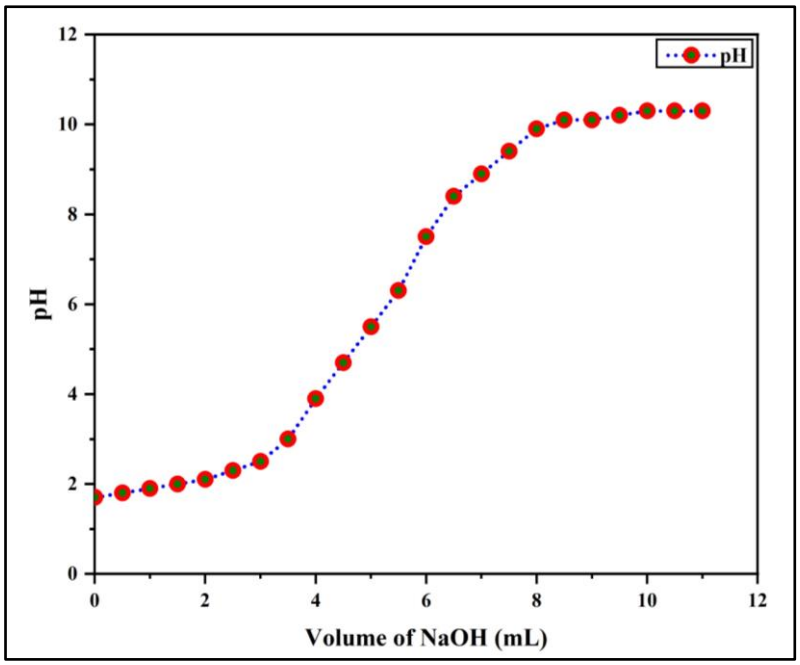

Figure 6.2. pH titration curve of Sn-ATMP.

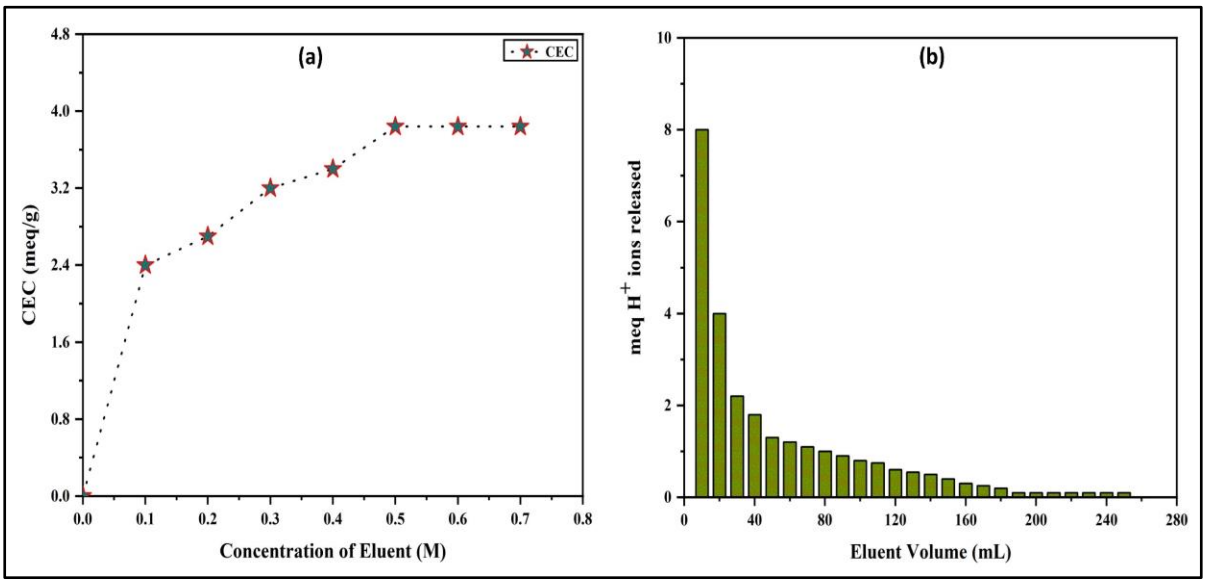

Figure 6.3. (a) Concentration and (b) Volume optimization for determination of CEC using Sn-ATMP.

6.3.2. Instrumental characterization of Sn-ATMP adsorbent

Inductively coupled plasma atomic emission spectroscopy (ICP-AES) elemental analysis of Sn-ATMP reveals Sn = 21.21% and P = 13.05%. C = 7.49%, H = 3.34%, and N = 2.63% are the outcome of the CHN analysis.

Sn-ATMP has been extrapolated as $Sn(C_3H_{12}NP_3O_9).5H_2O$ based on ICP-AES and CHN data, in accordance with previous research on metal phosphonates [35]. **Figure 6.4** displays of energy dispersive X-ray spectroscopy (EDX) graphs of the produced Sn-ATMP ion exchanger, which unambiguously demonstrate the presence of Sn and P in the exchanger.

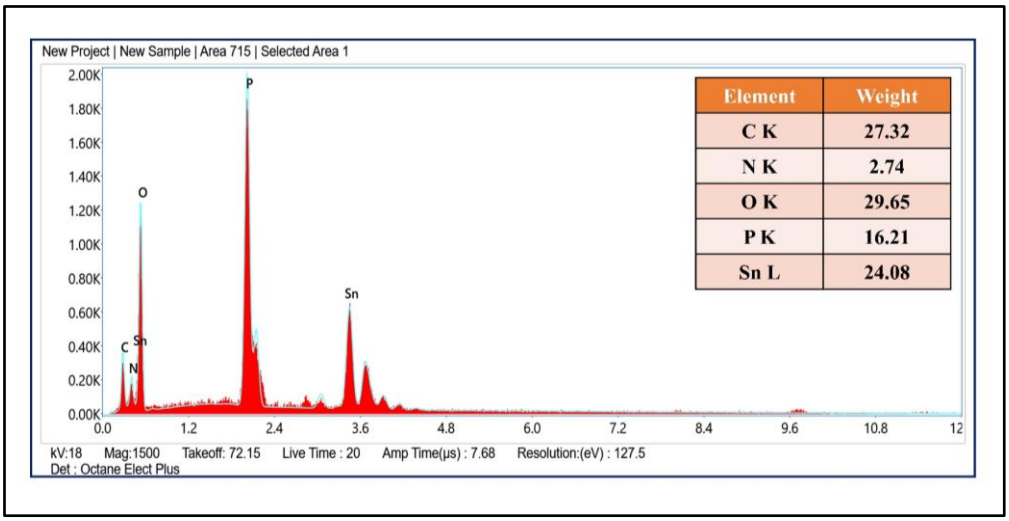

Figure 6.4. EDX spectra and table of Sn-ATMP.

The FTIR spectrum of tin phosphonate beforehand and after the adsorption of MB, MG, CV, RHB are displayed in **Figure 6.5**, respectively. Numerous sorption peaks are visible in the 4000-500 cm^{-1} wavenumber region, as shown by the FTIR spectra analysis, highlighting the intricate composition of the material under investigation. Before adsorption of dye on adsorbent, the intense and broad adsorption band at about 3525 cm^{-1} corresponded to the stretching mode of free water and surface -OH groups adsorbed on the adsorbent. Defective P-OH groups are another way for these ideas. One peak, centered at 1165 cm^{-1} and attributed to the C-N stretching vibration, and another, around 1060 cm^{-1}, were found to be correlated with the P-O-Sn stretching vibrations, respectively, splitting the broad band around 1000-1200 cm^{-1}. The cause of aquo H-O-H bending is a sharp medium band at approximately 1,625 cm^{-1}. Occurring C-H bending of CH_2 groups, P-C stretching vibrations, and the presence of tertiary amine are the causes of the band at approximately 1,438 cm^{-1} [30]. After adsorption of MB,

MG, CV and RHB dyes, the peaks were displaced, indicating the potential for interaction between the dyes and the synthetic ion exchanger. FTIR inspection revealed that ATMP coupling groups were uniformly distributed across the hybrid network and that Sn-ATMP's surface contained a significant number of hydroxyl groups, which could behave as places that the cationic dye could interact with.

The elimination of hydrated water and the condensation of -OH groups, which indicate the existence of protonic sites, resulted in a drop in CEC values as the calcination temperature grew [36]. The calcined samples' FTIR spectra **(Figure 6.6)** support the above observations, which can be most effectively explained as the loss or weakening of the peaks at around 3200 – 3550 cm^{-1} and 1625 cm^{-1}, which are attributed for the −OH group.

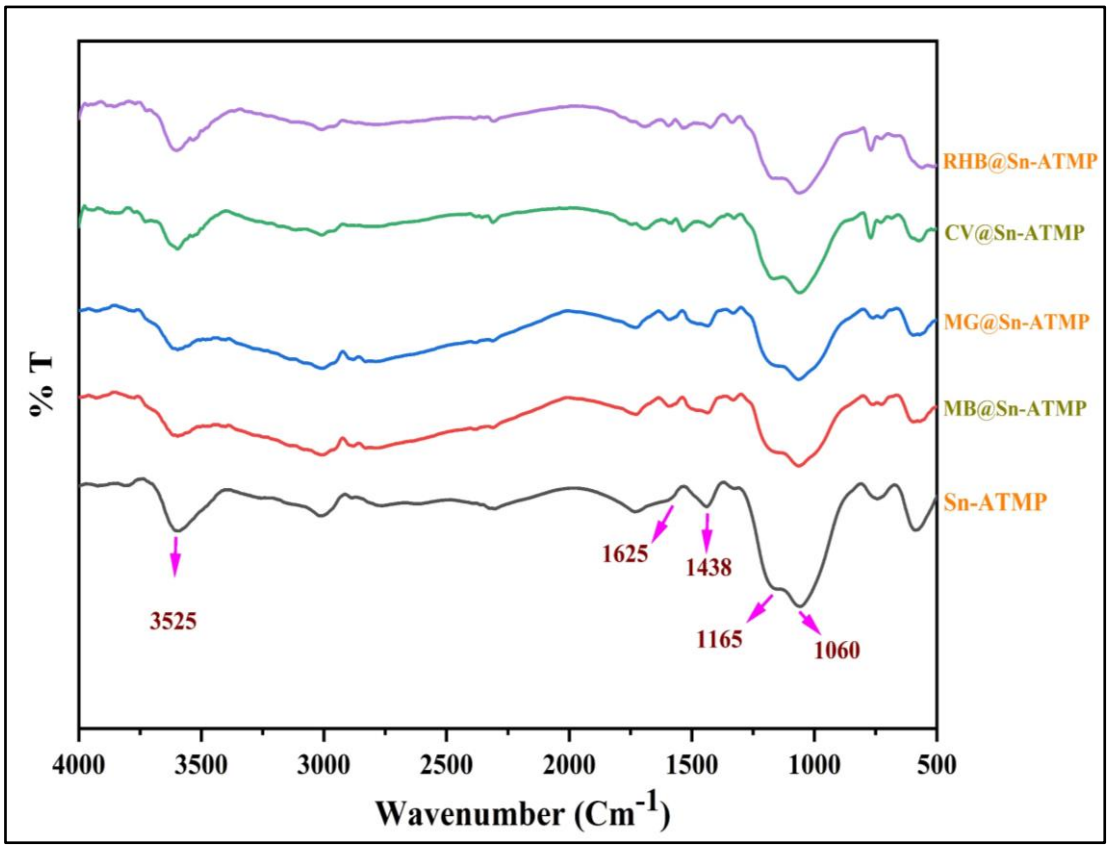

Figure 6.5. FTIR of Sn-ATMP and after sorption of dyes on Sn-ATMP.

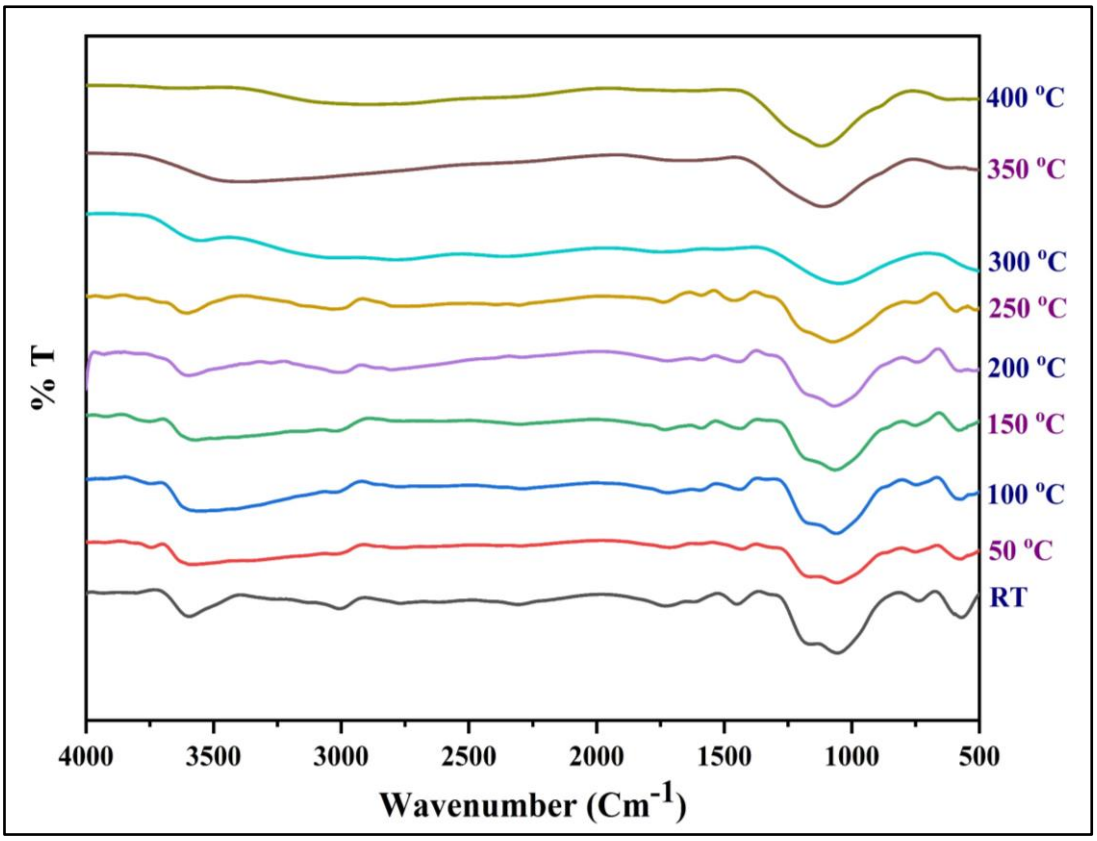

Figure 6.6. FTIR of Calcined graph of Sn-ATMP.

SEM (scanning electron microscopy) was used to evaluate the surface appearance of Sn-ATMP. Impressions of the Sn-ATMP surface captured either before or after the adsorption of dyes (MB, MG, CV, and RHB) are displayed in **Figure 6.7 (a-e)**, consecutively. Before adsorption, Sn-ATMP was recognized in **Figure 6.7 (a)** as having a rough surface with apparent pores and voids. However, **Figures 6.7 (b–e)** demonstrated that a significant amount of each dye (MB, MG, CV, RHB) was deposited on the Sn-ATMP surface's pores. The voids were indeed totally occupied with dye on adsorption.

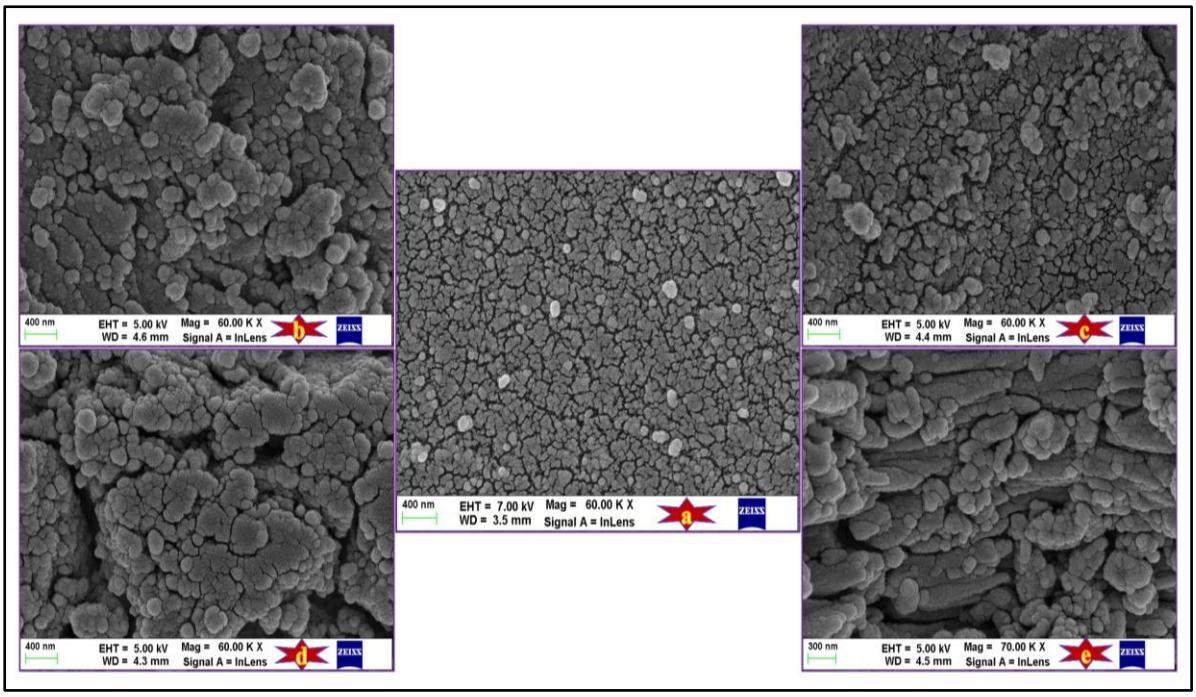

Figure 6.7. SEM images of (a) Sn-ATMP (b) MB@Sn-ATMP (c) MG@Sn-ATMP (d) CV@Sn-ATMP (e) RHB@Ce-ATMP.

X-ray diffraction patterns of Sn-ATMP and after adsorption with MB, MG, CV and RHB dyes indicates that all are amorphous in nature because of the absence of sharp peaks (**Figure 6.8**).

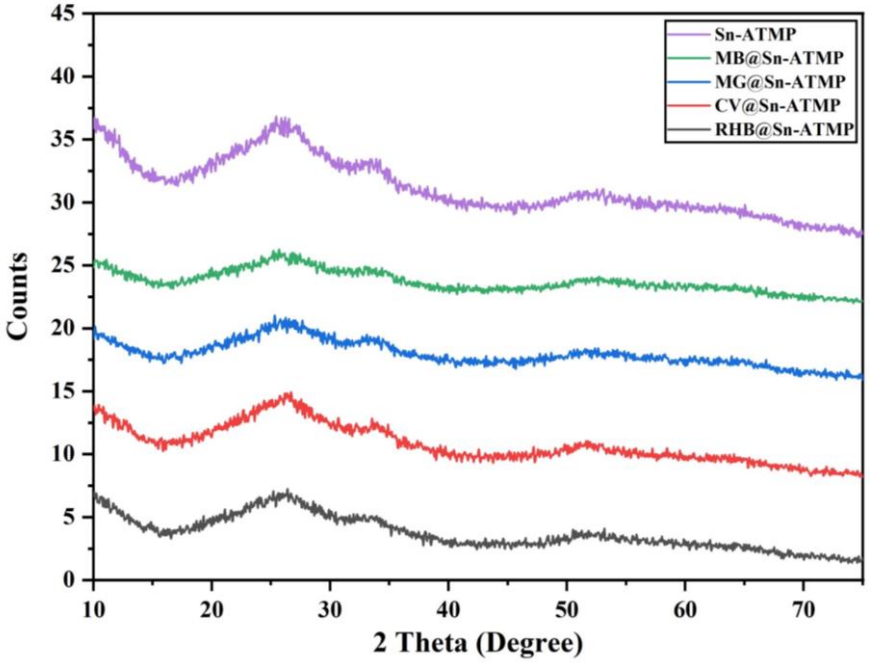

Figure 6.8. XRD Curve of Sn-ATMP.

The TGA curves of Sn-ATMP as-fabricated are displayed in **Figure 6.9**. The elimination of the physically adsorbed water caused a weight loss of 9.6% below 300 ^{0}C, and the breakdown of organic groups from ATMP was responsible for a 11.5% weight loss between 300 to 700 ^{0}C [37].

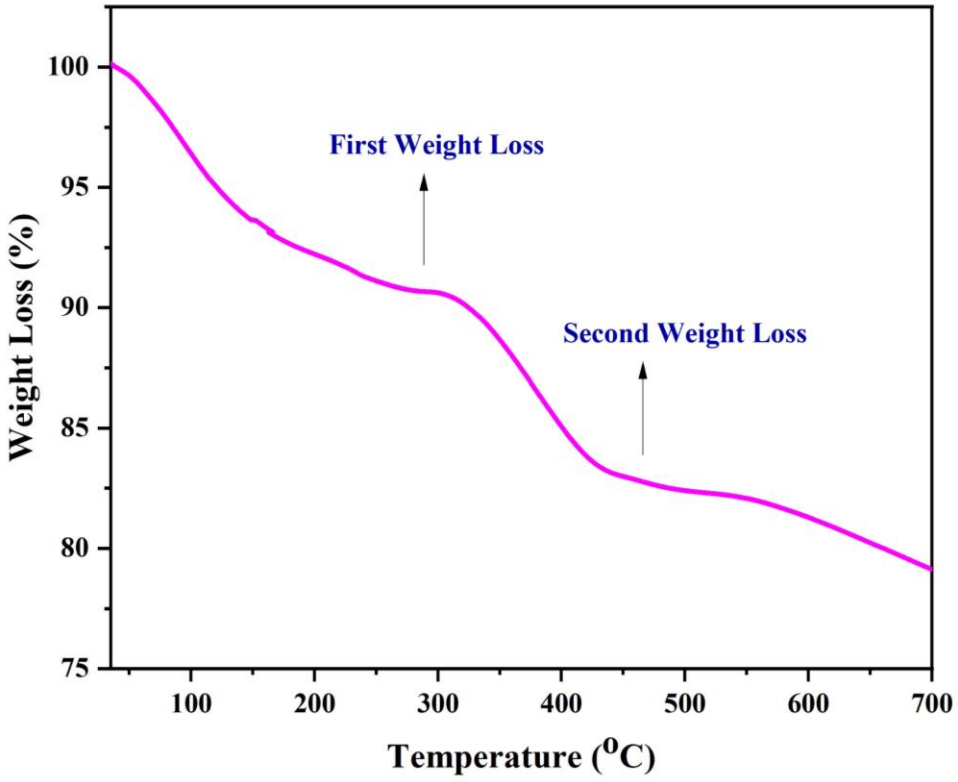

Figure 6.9. TGA Curve of Sn-ATMP.

6.3.3. Influence of parameters on dye adsorption efficiency

6.3.3.1. Effects of the solution's initial pH

One of the most significant aspects influencing the entire process of adsorption is the solution's pH since it has an enormous impact on the molecular and electrostatic interactions within the adsorbent and the molecules of dye. Adsorption of other ions can be influenced by the solution's pH because the hydroxyl and hydrogen ions are readily adsorbed. In relation to all other conditions (MB, MG, CV, RHB dye concentration (50 ppm), adsorbent dose (0.1 g), and solution temperature (298 K), time (60 min)) the impact of pH fluctuation on removal (%) was investigated across a pH range of 2 to 11. The dye solution's pH was adjusted using HCl and diluted NaOH. According to **Figure. 6.10,** a rise in pH initially causes an increase in the elimination of MB, MG, CV, and RHB; still an increase in pH eventually causes a decreasing

pattern. Adsorption of cationic dye onto the adsorbent surface is inhibited in acidic solutions owing to the excess concentration of H^+ ions. The quantity of OH^- ions in the solution rises with increasing pH. The decline in adsorption efficiency is caused by the cationic dyes' reaction with the OH^- ions in the solution to create a complex rather than adsorb on the adsorbent's surface [38,39]. As a result, according to the trials, the original MB, MG, CV, and RHB mediums exhibited an acidic (natural) pH, and this assertion was remained throughout the other experiments.

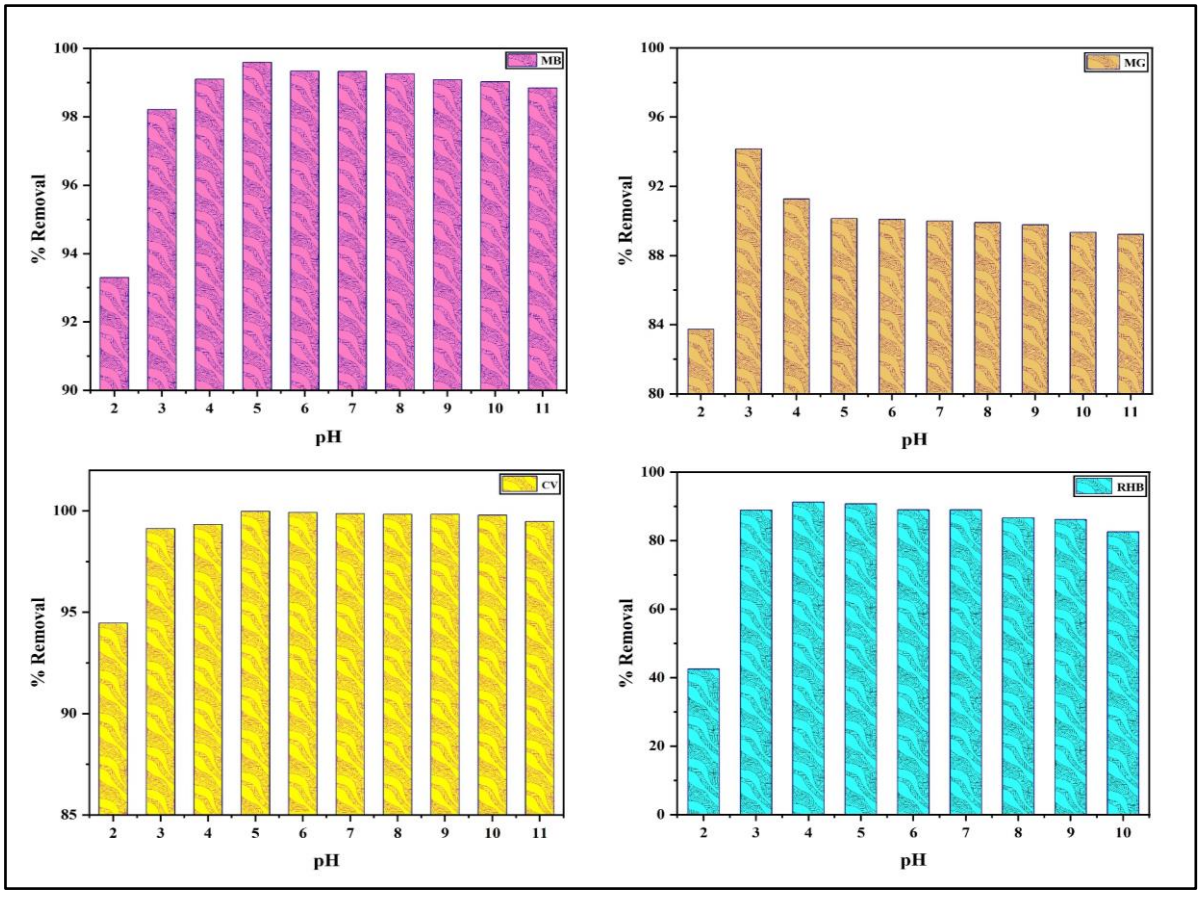

Figure 6.10. Effect of pH for after sorption of MB, MG, CV and RHB.

6.3.3.2. Effects of the adsorbent's dose

Proper selection of the adsorbent dose has been determined to have an essential role in controlling the efficiency of adsorption process because it is related directly to the area of surface and sites available for adsorption. In general terms, the percentage of dye removal rises as adsorbent mass and number of adsorption sites on adsorbent surface increase [40, 41].

The optimum dose of Sn-ATMP adsorbent for eliminating MB, MG, CV and RHB dyes were achieved by studying the effect of adsorbent dosage, which was 10-200 mg with the concentration of 50 ppm, solution temperature of 298 K, time of 60 min and optimum acidic pH on each dye's adsorption. **Figure 6.11** illustrates the findings. A percentage of MB, MG, CV and RHB adsorption increased sharply with the upgrade of adsorbent dose (from 10 to 80 mg). This elevation is likely resulting from the enlargement of special surface and accessibility of more adsorbent sites. Besides, further elevation in the quantity of adsorbent dose, from 80 to 200 mg, may be linked to the agglomeration of adsorbent particles and improvement of the removal efficiency percentage. After this, the removal efficiency remained unchanged. These results regarding the adsorption of MB, MG, CV and RHB dyes match with those obtained by other researchers [42]. Therefore, the adsorbent dose of 80 mg L^{-1} was selected for succeeding experiments.

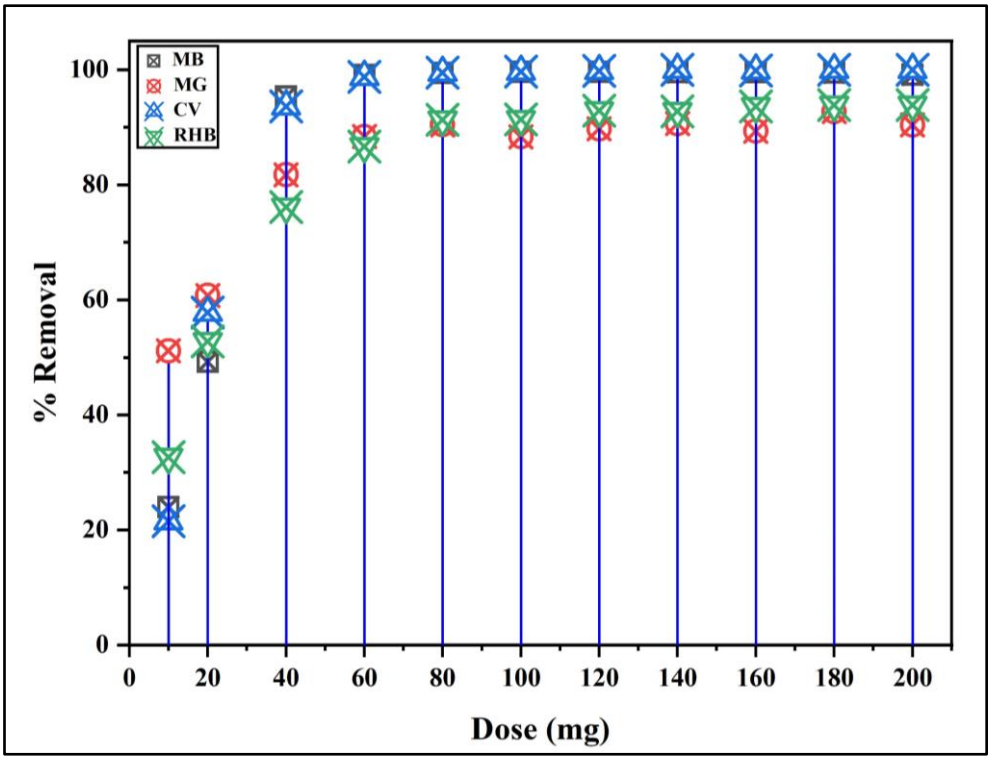

Figure 6.11. Effect of dosage of after sorption of MB, MG, CV and RHB.

6.3.3.3. Effects of initial dyes concentration

The dye concentration and the sites on the adsorbent surface are directly correlated with the impact of the initial dye concentration. The initial concentration of adsorption is a vital characteristic of the adsorption study [43].

The impact of the initial dye concentration of MB, MG, CV and RHB dyes in the solution (MG and RHB (10-250 ppm) and (MB and CV (10-250 ppm)) at 25^0C, time (60 min), optimum dose and at natural (Optimal) pH on its adsorption by Sn-ATMP were investigated. The impact of various initial dye concentrations on the adsorption onto Sn-ATMP is illustrated in **Figure 6.12**. The presented results could be noticed that, the removal percentage of MB, MG, CV and RHB dyes have been decreased by raising the initial dye concentration, resulting in the adsorbent surface's adsorption sites becoming saturated [44,45]. The findings indicated that 50 ppm of dye was the greatest percentage of dye removal that could be achieved.

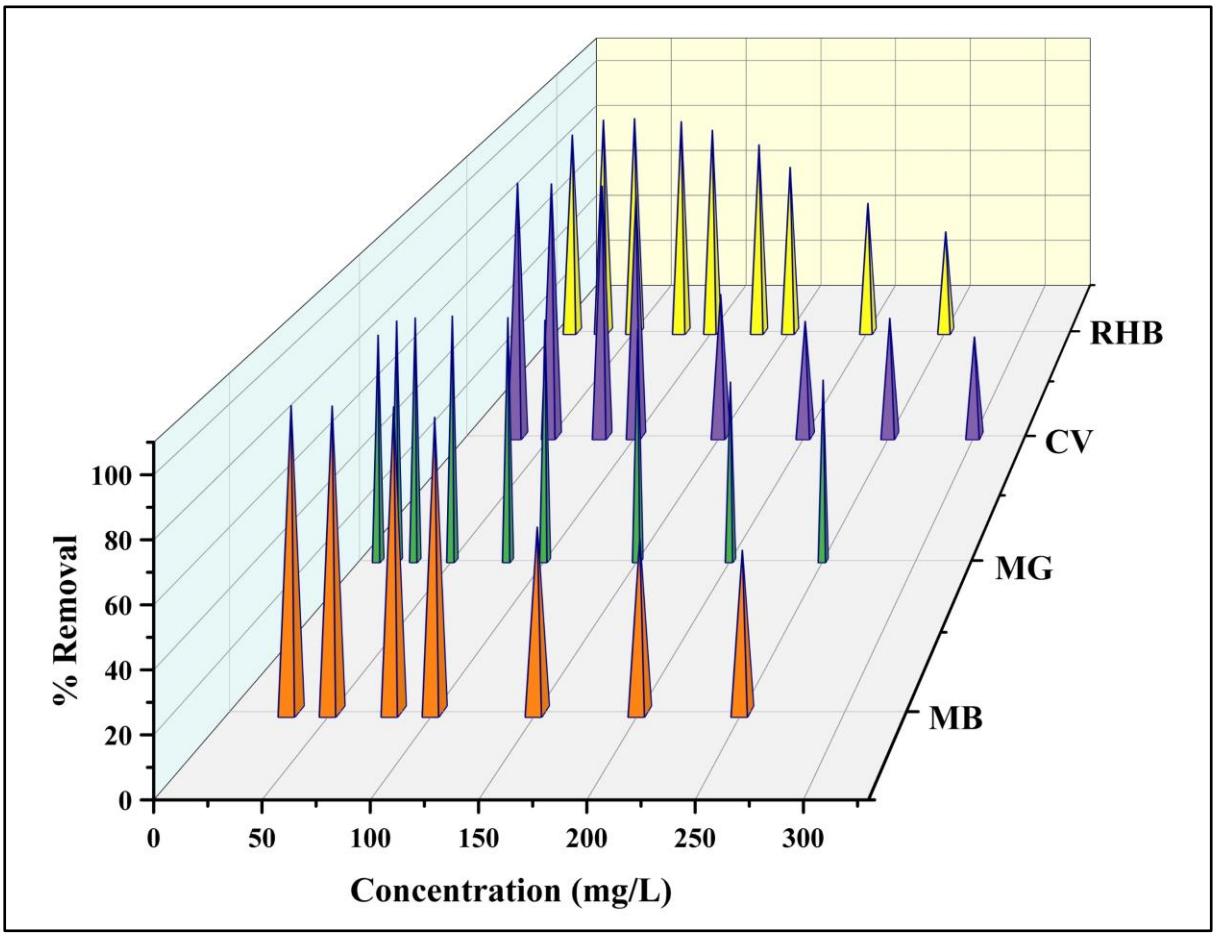

Figure 6.12. Effect of concentration of after sorption of MB, MG, CV and RHB.

6.3.3.4. Effects of contact time

In the adsorption process, one crucial factor is the duration of contact between the adsorbent and the adsorbate [46]. Here, the adsorption of MB, MG, CV and RHB was followed over the time using Sn-ATMP, while keeping the other parameters at constant values (adsorbent dose: 80 mg, dye concentration: 50 ppm, natural pH, and temperature: 298 K). **Figure 6.13**

and Figure 6.14 show the effects of the contact time (5-360 min) on the dye removal (%) of adsorbents, respectively. **Figure 6.15 and Figure 6.16** show the UV-vis adsorption spectrum for each dye sorption on Sn-ATMP.

Generally, on increasing the contact time, the removal efficiency increases and reaches a constant value at equilibrium state [40, 47]. The fast adsorption rate at the initial stage may be emphasized by the improved availability in the number of binding sites that are active on the adsorbent surface, Moreover, above equilibrium times, the percent removal of adsorbed dye is not significantly affected because of the adsorbents' active sites being saturated [48]. These results regarding the sorption of MB, MG, CV and RHB dyes match with those obtained by other researchers [49]. Accordingly, the removal efficiency was increased up to 50 min for MB, MG dyes and 60 min for CV, RHB dyes of contact time, after which, the equilibrium of sorption was attained.

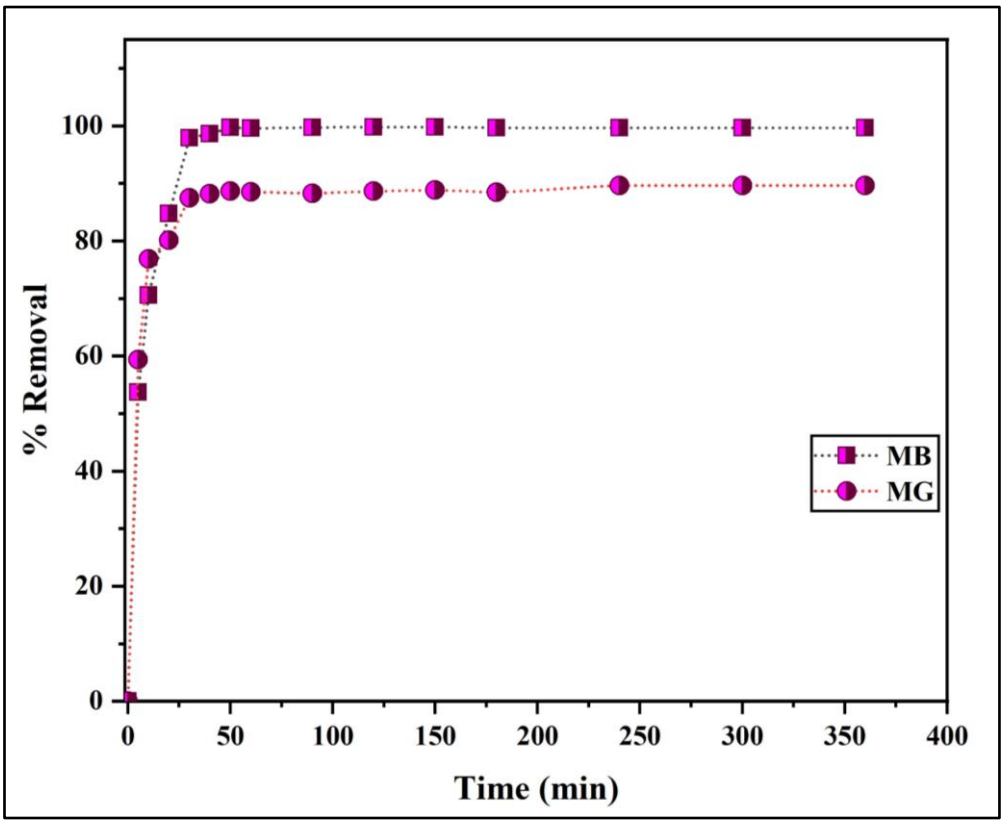

Figure 6.13. Effect of time of after sorption of MB and MG.

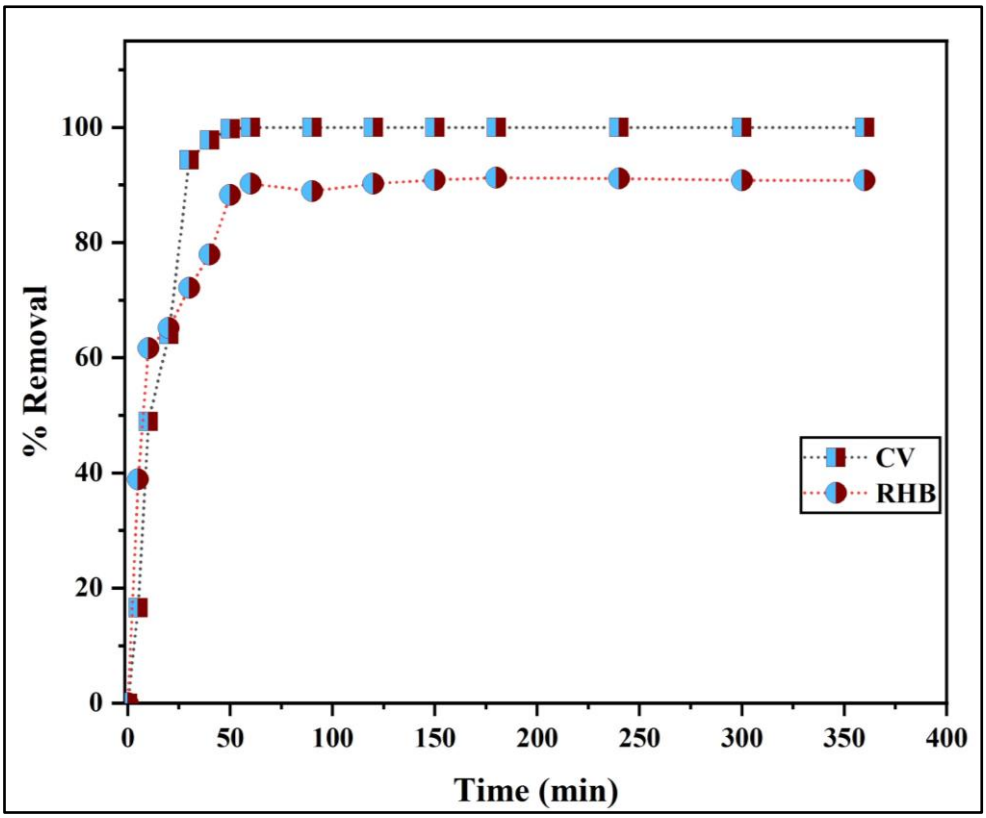

Figure 6.14. Effect of time of after sorption of CV and RHB.

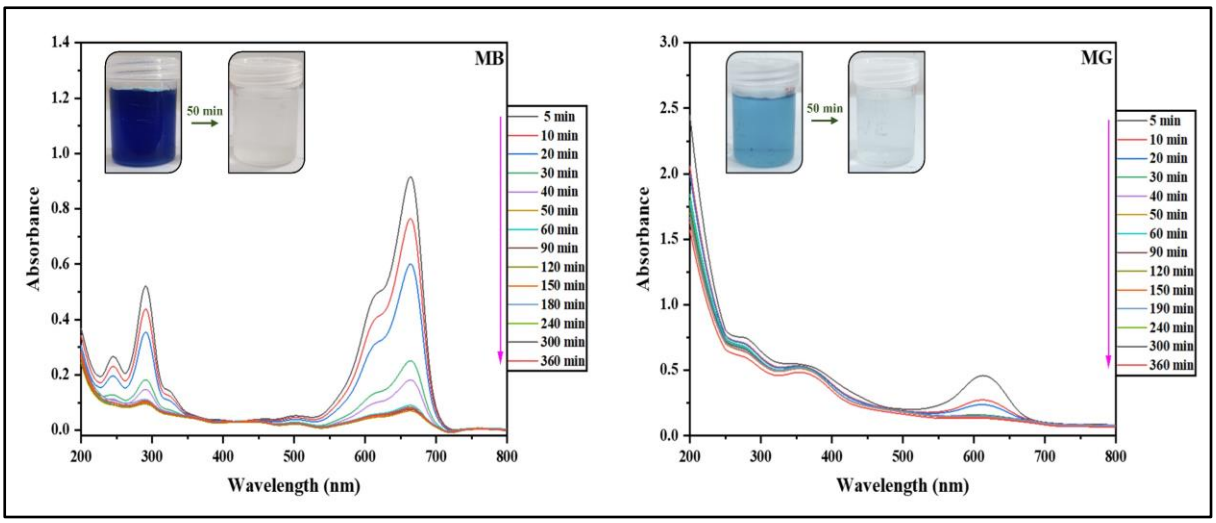

Figure 6.15. UV-vis adsorption spectra for After sorption of MB and MG.

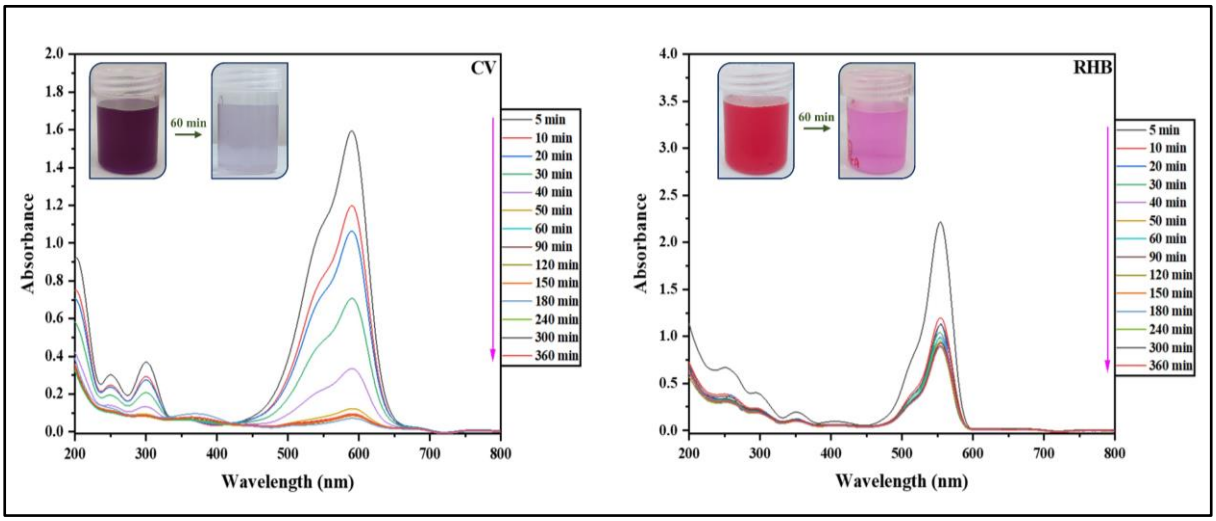

Figure 6.16. UV-vis adsorption spectra for After sorption of CV and RHB.

6.3.3.5. Effect of temperature

The temperature is among the most essential factors in determining the adsorption process. Investigating the impact of temperature on the sorption process was done at four distinct temperatures (25, 40, 50 and 60^0C) at natural pH, using 80 mg of adsorbent dose, contact time (50 min for MB and MG), (60 min for CV and RHB) and 50 ppm dye solutions. As shown in **Figure 6.17,** The adsorbed quantity of MB, MG, CV and RHB dyes decreased by rising the temperature. It is indicated that the adsorption process is exothermic if the number of adsorption sites decreases with temperature increases [50]. Similar results were observed in [51].

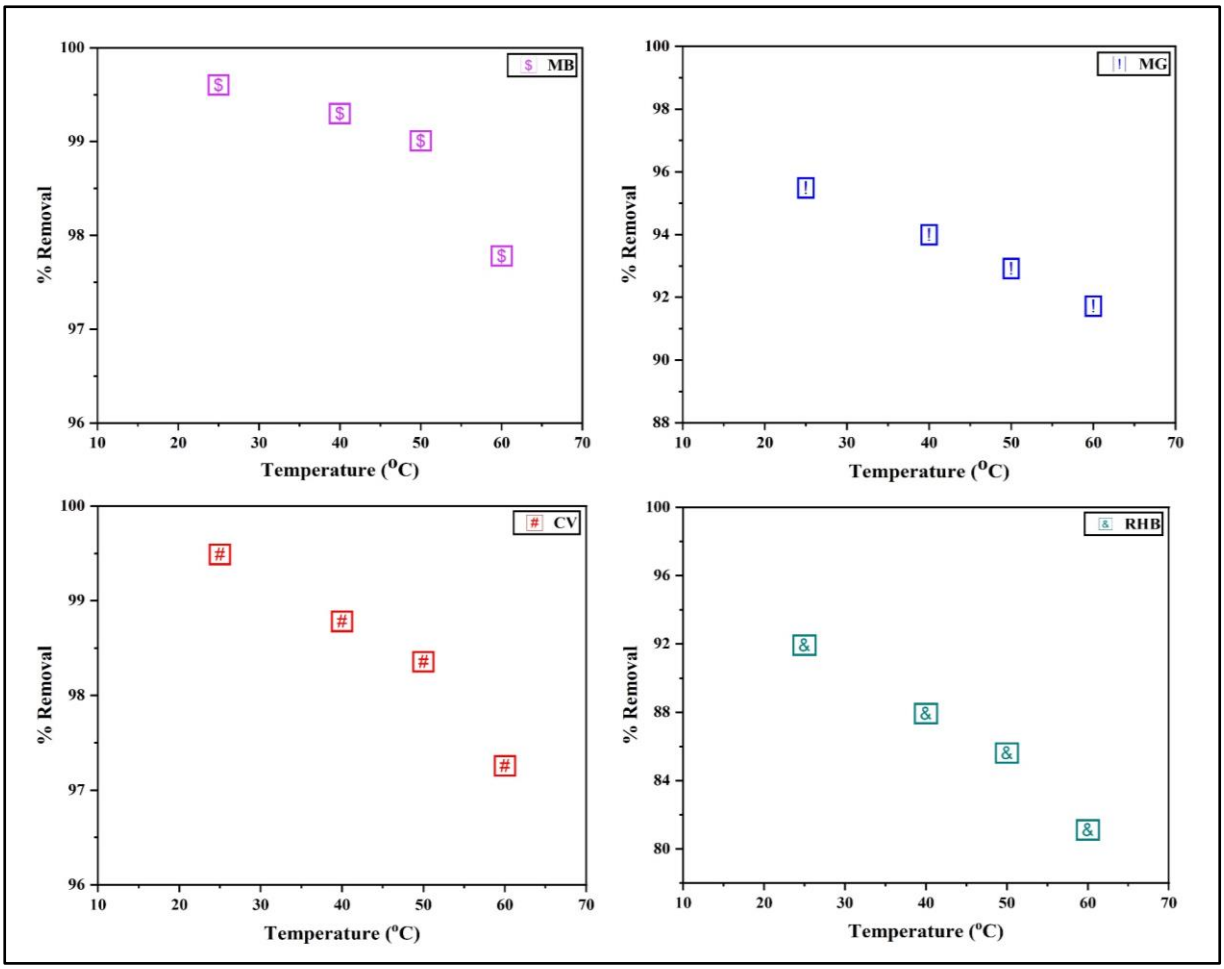

Figure 6.17. Effects of temperature of after sorption of MB, MG, CV and RHB on Sn-ATMP.

6.3.4. Kinetics models

The sorption rate is an essential factor for examining the adsorption property of an adsorbent. The correlation coefficients (R^2), which show which experimental data best suited the model, are one of the most crucial factors in determining the kinetic models [52]. **Figure. 6.18, Figure. 6.19 (a and b)** and **Figure. 6.20** shows the linear curves of the pseudo-first-order, pseudo-second-order and intraparticle diffusion kinetic model for adsorption of MB, MG, CV and RHB dyes on Sn-ATMP respectively. The adsorption process's matching fitting curve's slope and intercept were used to derive the values of the kinetic parameters, which are shown in **Table 6.2**. Results show that the pseudo-first-order model fails to correlate appropriately the adsorption kinetics with low regression coefficient, whereas the correlation coefficients values (R^2) obtained for the pseudo-second-order model were highest ($R^2 = 0.999$) and the calculated adsorption capacities were extremely close to the experimental ones (**Table 6.2**), illustrating that the pseudo-second-order kinetic model best fits the kinetics data. Similar results were observed by other researchers [53].

If the diffusion mechanism is controlled by intra-particle diffusion, then the intercept C should cross the origin. As per the Weber-Morris model, but as shown in **Figure. 6.20 and Table 6.2** all the intercepts are nonzero i.e. not crossing the origin; thus, it showed that intra particle diffusion is not rate limiting [53].

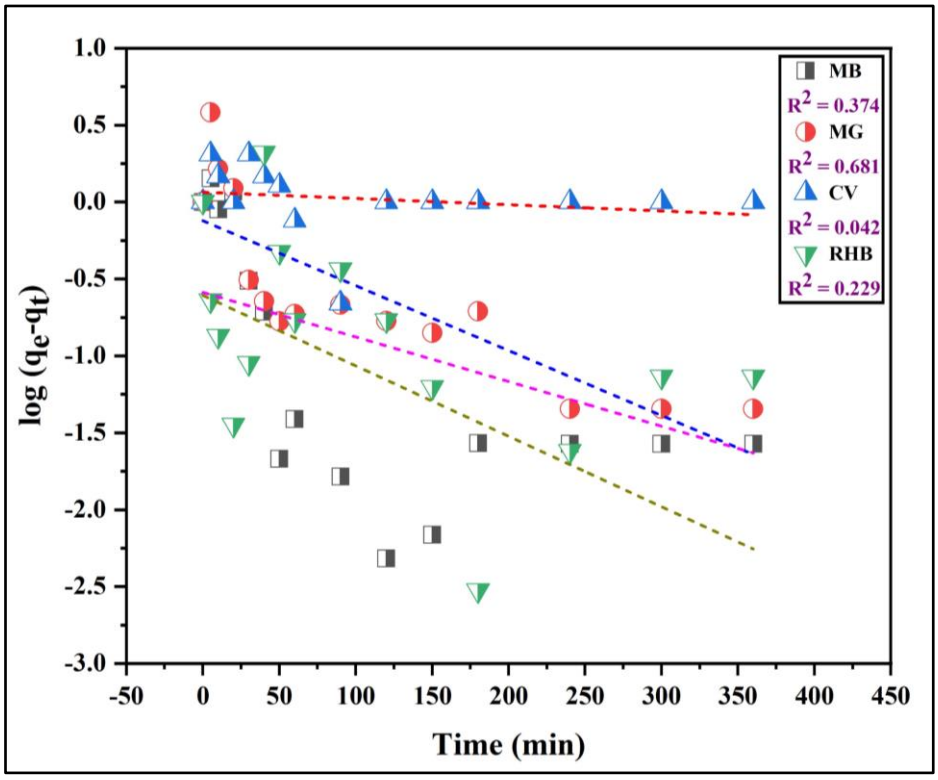

Figure 6.18. pseudo-first-order kinetic models for sorption of MB, MG, CV and RHB dyes on Sn-ATMP

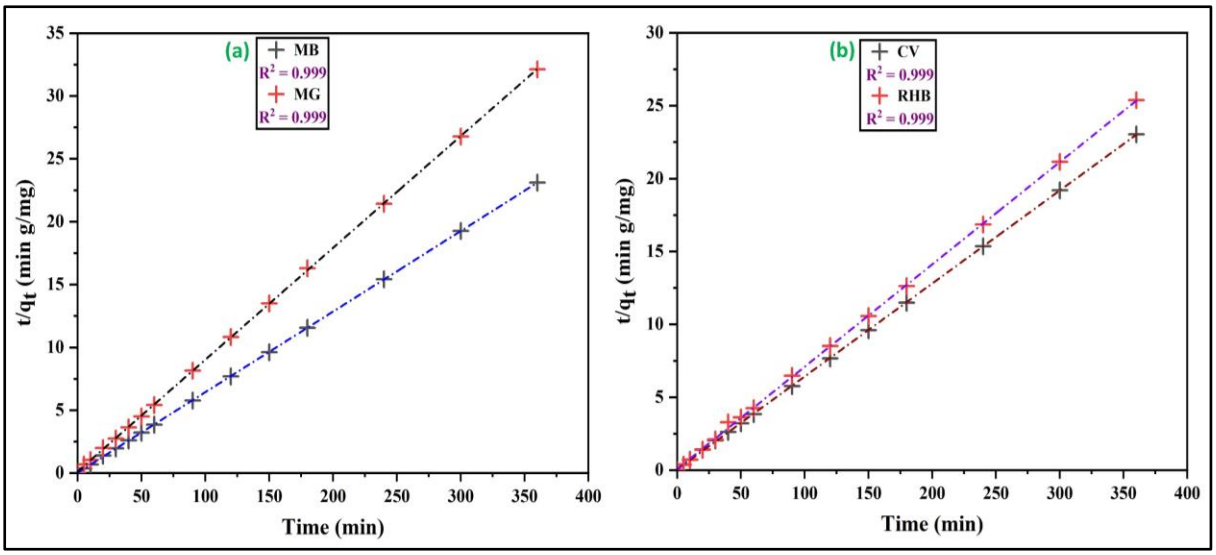

Figure 6.19. Pseudo-second-order kinetic models for sorption of (a) MB and MG (b) CV and RHB dyes on Sn-ATMP.

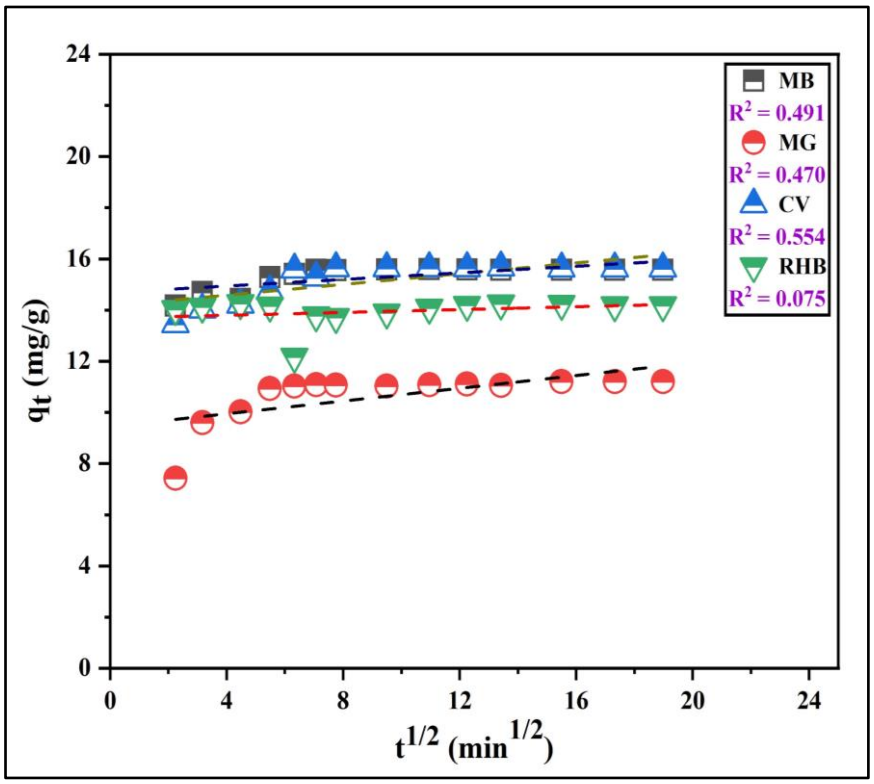

Figure 6.20. Infraparticle diffusion kinetic models for sorption of MB, MG, CV and RHB dyes on Sn-ATMP.

6.3.5. Adsorption equilibrium isotherms

The equilibrium of adsorption isotherm is an essential model for explaining the behavior of adsorption. Adsorption isotherms, method used to calculate the quantity of solute adsorbs per unit of adsorbent, as a function of temperature-dependent equilibrium concentration. This result is significant to appreciate the adsorption behaviour to identify the most suitable adsorption isotherm model [43,44]. The present investigation examined Langmuir and Freundlich adsorption isotherms at 25°C to identify the sort of interaction that occurs between Sn-ATMP and the dyes MB, MG, CV, and RHB **(Figures 6.21 – Figure 6.24)**.

6.3.5.1. Isotherm of Langmuir

The finest adsorption isotherm for solute adsorption is the Langmuir adsorption isotherm, which is crucial in figuring out the adsorbent's maximal capacity [51].

The graph (**Figure 6.21 and Figure 6.22**) shows linear patterns for the MB, MG, CV and RHB. The values of Q_{max} and K_L, which are given in **Table 6.2**, have been calculated using the slope and intercept of the straight lines in the plot of $1/q_e$ against $1/C_e$. The Langmuir model effectively describes the sorption data with R^2 values of 0.967, 0.968, 0.917, and 0.951. The Langmuir model, which assumes a monolayer and uniform coverage at the surface of Sn-ATMP, is shown to be applicable when such high coefficient values are obtained. Furthermore, the corresponding dimensionless constant separation factor (R_L) values were 0.01, 0.37, 0.007, and 0.06. Thus, these findings demonstrate that adsorption is more favorable. It shown that the adsorption of MB, MG, CV and RHB on Sn-ATMP perfectly fits the Langmuir equilibrium isotherm. In the current present investigation, maximal MG sorption capacity towards Sn-ATMP is 66.66 $mg.g^{-1}$. Similarly work has been done on GO/cellulose bead composite towards adsorption of MG is 17.86 $mg.g^{-1}$ [55].

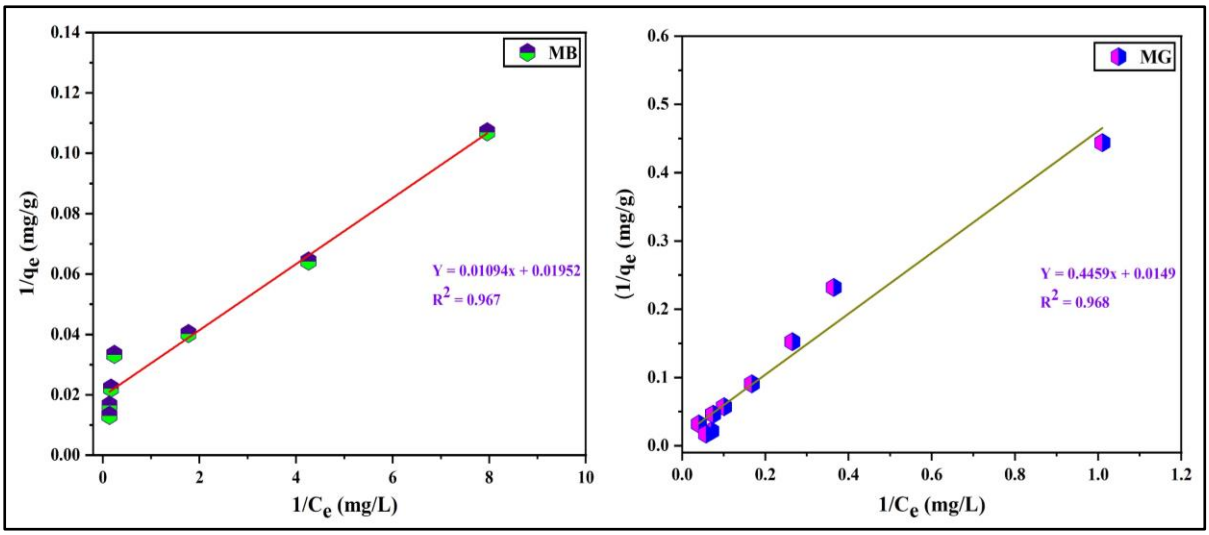

Figure 6.21. Langmuir adsorption isotherm model for MB and MG.

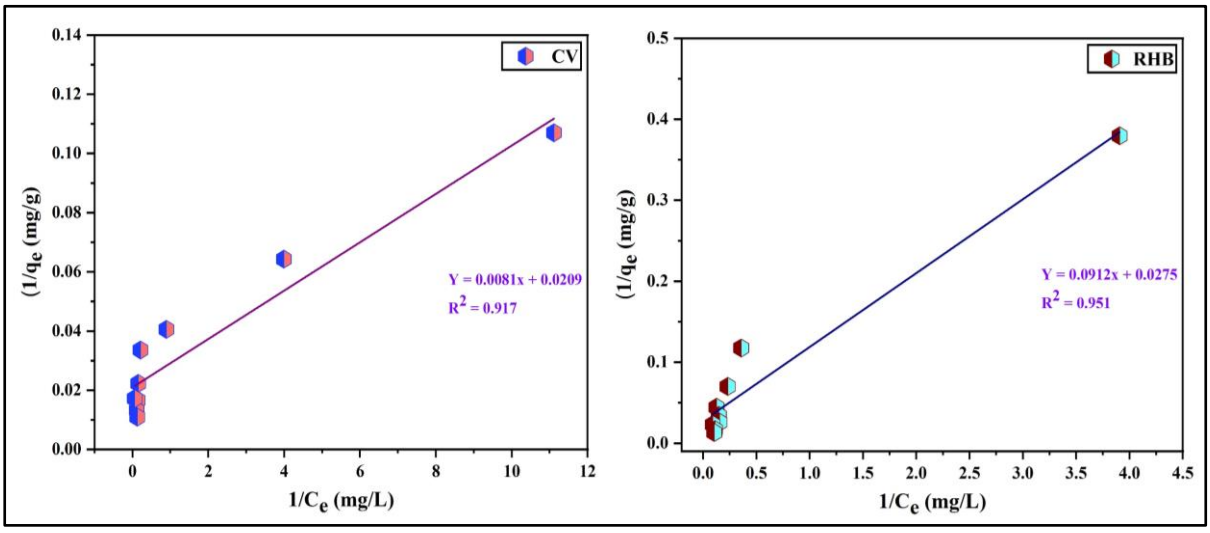

Figure 6.22. Langmuir adsorption isotherm model for CV and RHB.

Table 6.2. Linear Langmuir Isotherm Model Parameters for Adsorption Process at 298 K.

Dyes	Langmuir constants			
	R^2	K_L ($L.mg^{-1}$)	Q_{max} ($mg.g^{-1}$)	R_L
MB	0.967	1.788	51.28	0.011
MG	0.968	0.033	66.66	0.372
CV	0.916	2.679	46.08	0.007
RHB	0.951	0.302	36.23	0.061

6.3.5.2. Isotherm of freundlich

The Freundlich isotherm was utilized to fit the experimental data of equilibrium. The Freundlich isotherm curve of MB, MG, CV and RHB is shown in **Figure 6.23 and Figure 6.24.** MB (0.892), MG (0.910), CV (0.881) and RHB (0.909) revealed the correlation coefficient (R^2) values. The numerical values of the Freundlich equilibrium coefficients K_F and n were generated from the graph of sorption data. The parameter 1/n is a determine of sorption intensity or surface heterogeneity with values across 0 and 1 becoming more heterogeneous as the value number approaches to zero [39]. **Table 6.3** depicts the obtained parameters of the Freundlich isotherm. The numerical values of 1/n (MB (0.40), MG (1.01), CV (0.41) and RHB (0.79)) give an indication of the favorability of adsorption, more heterogenous and high tendency of MB, MG, CV and RHB for the adsorption onto Sn-ATMP.

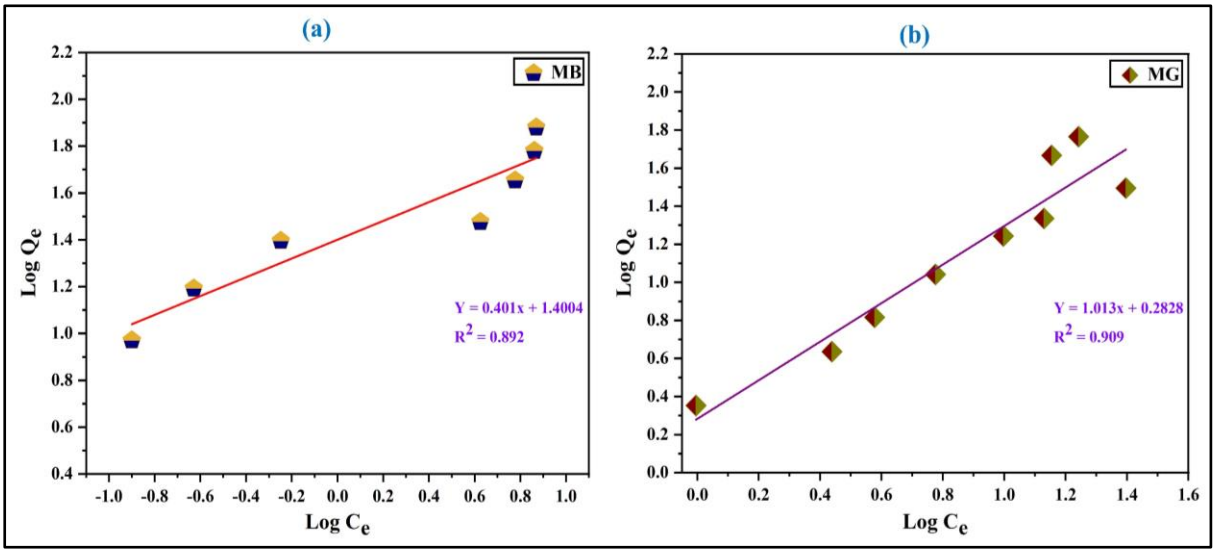

Figure 6.23. Freundlich adsorption isotherms for (a) MB and (b) MG.

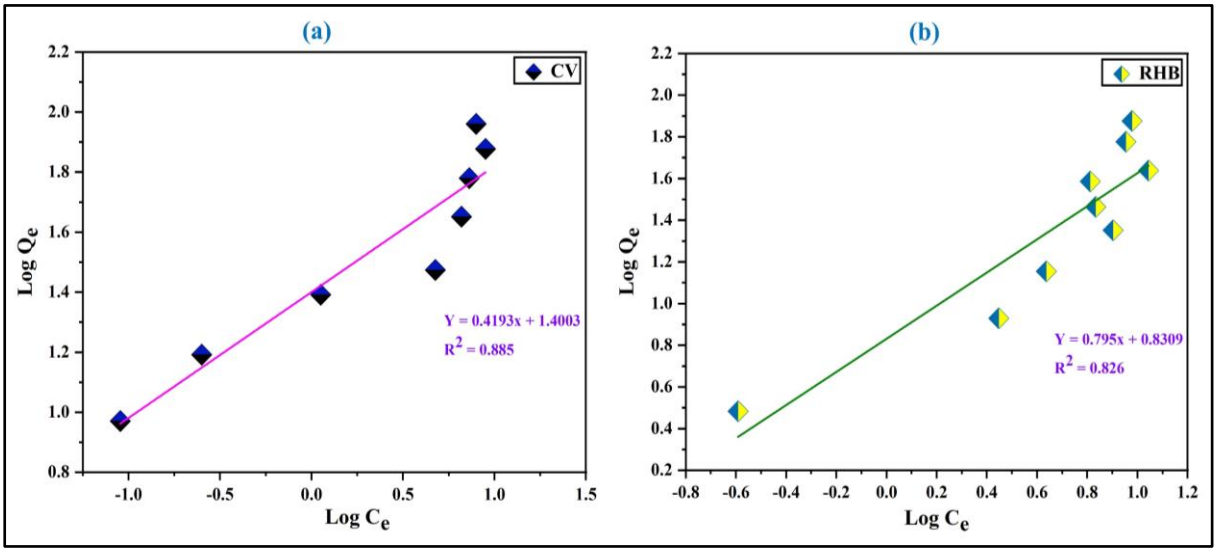

Figure 6.24. Freundlich adsorption isotherms for (a) CV and (b) RHB.

Table 6.3. Linear Freundlich Isotherm Model parameters for the Adsorption process at 298 K.

Dyes	Freundlich constants		
	R^2	K_f (mg.g^{-1})	n
MB	0.892	25.12	2.49
MG	0.909	1.917	0.98
CV	0.885	25.13	2.38
RHB	0.826	6.774	1.25

6.3.6. Adsorption thermodynamics

Thermodynamics studies give insight concerning the way variations in temperature affect the adsorption process, which might be elucidated by evaluating the thermodynamic parameters. The calculated thermodynamic parameters including Gibbs free energy change, enthalpy, and entropy change for the MB, MG, CV and RHB adsorption onto Sn-ATMP are listed in **Table 6.3**. **Figure 6.25** shows the plot of ln K_d versus 1/T, from which the values of entropy change (ΔS°) and enthalpy change (ΔH°) were obtained.

The ΔG° values were measured at 298, 313, 323 and 333 K. The respective negative values of ΔG°, which indicates that the adsorption technique of MB, MG, CV and RHB onto the Sn-ATMP is spontaneous, thermodynamically favorable at all temperatures tested here and also achievement of a more constant energy level after sorption. The negative enthalpy change (ΔH^0) for each dye reveals that the adsorption of MB, MG, CV and RHB on Sn-ATMP is exothermic process which correlates with the decrease of adsorption capacity by increasing temperature. Moreover, the entropy change(ΔS^0) is negative for the sorption of MB, MG, CV and RHB on Sn-ATMP which signifies that the mobility of MB, MG, CV and RHB on Sn-ATMP decreases after adsorption on Sn-ATMP. As the negative ΔS^0 is unfavorable for the spontaneous adsorption, the absence of disarray in the system [56].

Table 6.3. Thermodynamic parameters assessed at various temperatures using Sn-ATMP.

Dyes	Temperature (K)	ΔG° (kJ.mol^{-1})	ΔH° (kJ.mol^{-1})	ΔS° (J.mol^{-1}.°C^{-1})
MB	298	-10.80	-38.95	-93.64
	313	-9.860		
	323	-9.233		
	333	-7.256		
MG	298	-4.122	-15.23	-37.28
	313	-3.546		
	323	-3.188		
	333	-2.815		
CV	298	-10.16	-39.06	-97.20
	313	-8.407		
	323	-7.857		
	333	-6.657		
RHB	298	-3.141	-22.39	-64.57
	313	-2.138		
	323	-1.663		
	333	-0.813		

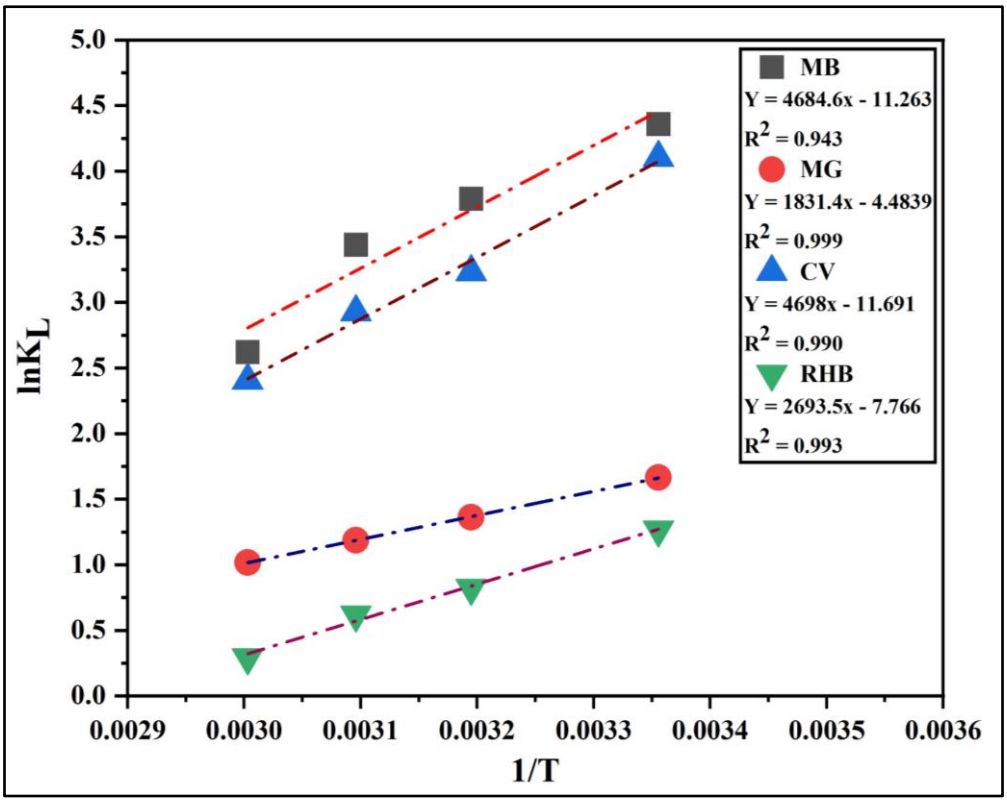

Figure 6.25. Thermodynamics for MB, MG, CV and RHB.

6.3.7. Desorption and Reusability of Sn-ATMP

The purpose of the desorption experiments is to gain information about the recovery of the adsorbent. Indeed, reusability of an adsorbent is very important from an economic perspective. To reduce costs and protect the environment, the adsorbents' renewal is vital [57]. The mechanism of the sorption process and the potential recovery of the adsorbent for future use could both be confirmed by the study of dye desorption. Therefore, the multiple adsorption-desorption experiments were performed. Owing to the structural hydroxyl groups present in Sn-ATMP, the dyes are most likely bonded by hydrogen bonds or weak van der Waals forces, which facilitates sorption and desorption.

Herein, the desorption of the MG@Sn-ATMP, CV@Sn-ATMP and RHB@Sn-ATMP was studied by using diverse eluting agents including 0.1 M EDTA solution for MG (50 min) and CV (60 min) and 0.05 M HCl solution for RHB (60 min). **Figure 6.26** displays the influence of adsorption-desorption cycles on the MG, CV and RHB removal efficiency (%). For this purpose, regeneration experiments have been performed in successive cycles. It has been found that the removal efficiency (%) of the adsorbent gradually decreases with an increasing recycle number of the adsorbent for the adsorption-desorption experiments, as

illustrated in **Figure 6.26**. The reduction in removal efficiency could be linked to the reduction of adsorbent sites and the blockage of pores. The adsorbents after desorption were washed by distilled water twice and dried at 50℃ in vacuum oven for 24 hrs for the next adsorption process. This result reveals that the interactions between MG, CV, RHB and Sn-ATMP are mostly created electrostatic attraction and could be easily desorbed to regenerate the adsorbent.

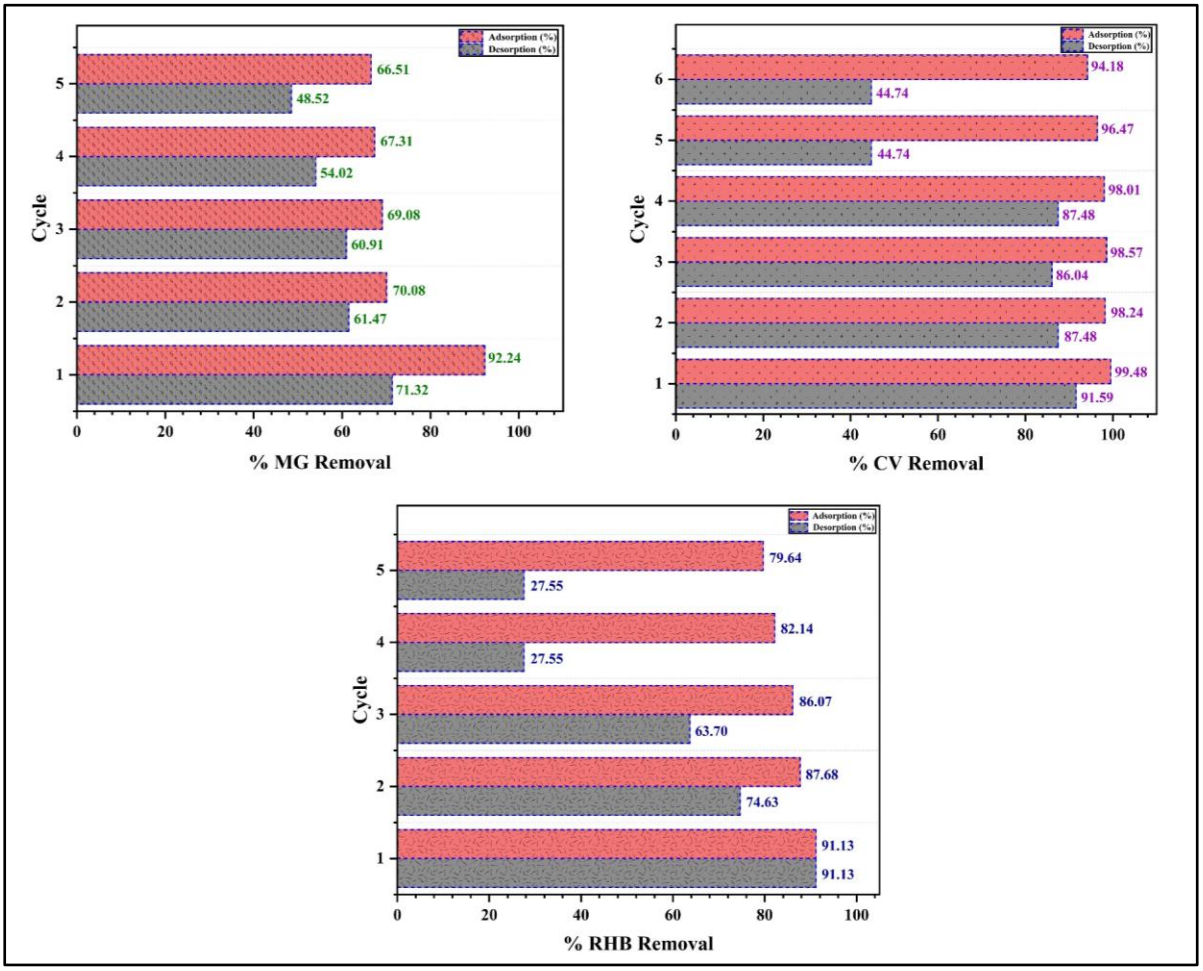

Figure 6.26. Adsorption-Desorption cycles of MB, MG, CV and RHB by using Sn-ATMP.

In the case of MB@Sn-ATMP, a 0.05 M HCl solution was used to desorption experiment, but it's not desorbed. Therefore, three time wash the MB@Sn-ATMP using 0.05 M HCl then regenerating adsorbents was washed with deionized water then dried. It had adsorbed the dye for 50 min in this work. The impact of seven consecutive adsorption cycles on MB adsorption by Sn-ATMP. In the first cycle, almost 99.4% of dyes were sorption on the adsorbent. In the subsequent cycles, the dye adsorption values slightly reduced from 99.3% to 70.1% for the 7th cycle (**Figure 6.27**). From the results, it can be established that the present adsorbent has excellent structural stability and recyclability without any substantial loss of activity.

Taken together, the Sn-ATMP exhibited superior reusability for MB, MG, CV and RHB removal, which made it a potential candidate for advanced treatment of dyeing effluents.

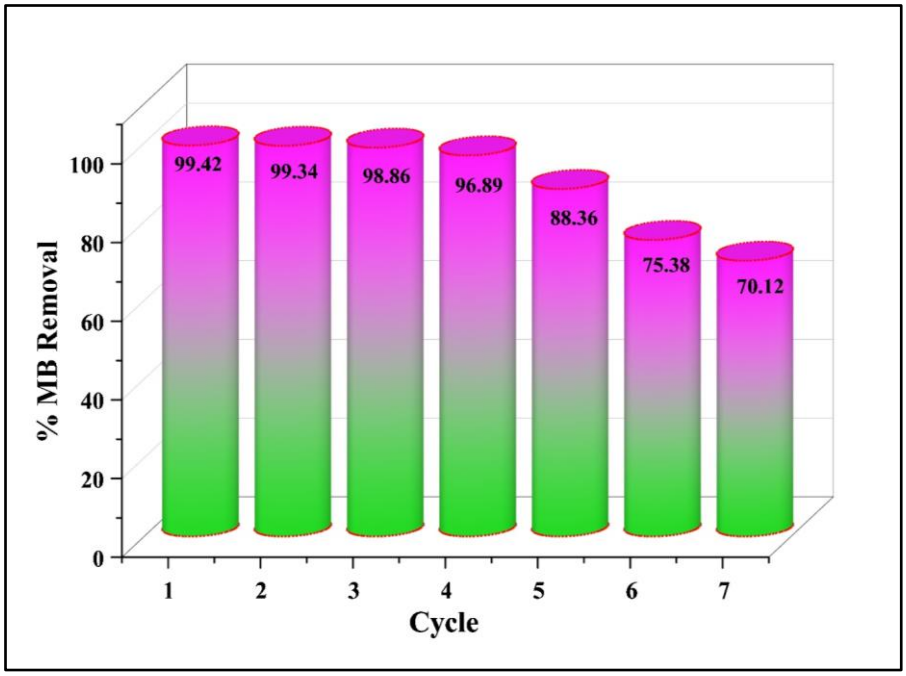

Figure 6.27. Regeneration Cycles of MB by Sn-ATMP.

6.4. Conclusion

Investigations have been conducted with cationic dyes (MB, MG, CV, RHB) adsorption onto Sn-ATMP. The material was characterized by ICP-CHN, FTIR, SEM, EDS, TGA, UV and XRD. Sorbent material Sn-ATMP, exhibits good chemical and thermal stability. Various impact factors such as solution's pH, adsorbent dosage, initial dye concentration, contact time and temperature were optimized. Maximum adsorption, at equilibrium (99.7% and 88.6%), has been achieved within the first 50 minutes of the contact, indicating superior absorptivity of Sn-ATMP for MB and MG. Maximum adsorption, at equilibrium (100% and 90.1%), has been achieved within the first 60 minutes of the contact, indicating excellent absorptivity of Sn-ATMP for CV and RHB. Getting, adsorption trend for the cationic dyes onto Sn-ATMP is, CV > MB > RHB > MG. The adsorption of MB, MG, CV and RHB by the Sn-ATMP fits the Langmuir equilibrium isotherm perfectly. The kinetics of MB, MG, CV, RHB adsorption on Sn-ATMP were found to fit the pseudo-second-order model. The sorption process was found to be spontaneous and exothermic, as demonstrated by the estimation of the thermodynamic parameters (ΔG^o, ΔH^o, ΔS^o). Eventually, Sn-ATMP may be regenerated after sorption of MB, MG, CV, RHB using HCl and EDTA. Overall, the adsorption experiments showed that Sn-

ATMP is an efficient adsorbent for the removal of cationic dyes and its prominent use in waste water treatment.

6.5. References

[1] L. Borah, M. Goswami, P. Phukan, J. Environ. Chem. Eng. **3(2)** (2015) 1018–1028.

[2] M. Sridevi, C. Nirmala, N. Jawahar, G. Arthi, S. Vallinayagam, V.K. Sharma, J. Mol. Struct. **1241** (2021) 130596.

[3] D.A. Yaseen, M. Scholz, Environ. Sci. Pollut. Res. **25(2)** (2018) 1980–1997.

[4] M. T. Yagub, T. K. Sen, S. Afroze, H. M. Ang, Adv. Coll. Interf. Sci. **209** (2014) 172–184.

[5] G. Uyar, H. Kaygusuz, F.B. Erim, React. Fun. Polym. **106** (2016) 1–7.

[6] P. Arabkhani, A. Asfaram, J. Hazard. Mater. **384** (2020) 121394.

[7] D. Xu, H. Ma, J. Clean. Prod. **313** (2021) 127758.

[8] D. Vara, S. Jha, S. Bisht, S. Shahabuddin, R. Gaur, S.I. Tyagi, Toxics **12** (2024) 266.

[9] Y. Chen, Y. Li, Y. Yu, Y. Li, K. Xia, Y. Wang, S. Li, J. Mater. Sci. **51** (2016) 7016.

[10] Saruchi, V. Kumar, Arab. J. of Chem. **12** (2019) 316-329.

[11] Z. Cai, Y. Sun, W. Liu, F. Pan, P. Sun, J. Fu, Environ. Sci. Pollut. Res. **24(19)** (2017) 15882–15904.

[12] S. Zhang, J.-Q. Jiang, M. Petri, Npj Clean Water **4(1)** (2021) 1.

[13] M.M. Hasan, M.A. Shenashen, M.N. Hasan, H. Znad, M.S. Salman, M.R. Awual, J. of Mol. Liq. **323** (2021) 114587.

[14] Y. Liu, F. Zhang, W. Zhu, D. Su, Z. Sang, X. Yan, S. Li, J. Liang, S.X. Dou, Carbon **160** (2020) 88–97.

[15] K. Maheria, U. Chudasama, Ind. Eng. Chem. Res. **46** (2007) 6852-6857.

[16] S. Rani, S. Chaudhary, Mater. Today Proc. **60** (2022) 336–334.

[17] J. Joseph, R.C. Radhakrishnan, J.K. Johnson, S.P. Joy, J. Thomas, Mater. Chem. and Phy. **242** (2020) 122488.

[18] M.M. Sabzehmeidani, M. Ghaedi, K. Dashtian, H. Abbasi-Asl, **300** (2021) 113707.

[19] V. Watwe, S. Kulkarni, P. Kulkarni, Indus. Crop. Prod. **195** (2023) 116449.

[20] S.A. Hamid, M. Shahadat, B. Ballinger, S.F. Azha, S. Ismail, S.W. Ali, S.Z. Ahammad, J. Saudi Chem. Soc. **24** (2020) 785–798.

[21] I. Liaquat, R. Munir, N.A. Abbasi, B. Sadia, A. Muneer, F. Younas, S. Noreen, Environ. Pollut. (2024)123922.

[22] A. Chumpiboon, K. Thongsubsai, T. Pongsiri, J.T. Knijnenburg, Y. Ngernyen, Engg. App. Sci. Res. **49(3)** (2022) 381–394.

[23] A. Clearfield, Progress in Inorganic Chemistry, John Wiley and Sons. New York, 1998.

[24] W.A. Siddiqui, S.A. Khan, Bull. Mater. Sci. **30** (2007) 43−49.

[25] A. Clearfield, Z.J. Wang, Dalton Trans. **7** (2002) 2937− 2947.

[26] S. Bauer, T. Bein, N. Stock, Inorg. Chem. **44** (2005) 5882−5889.

[27] Y. Zhu, T. Zhen Ren, Z. Yuan, New J. Chem. **38** (2014) 1905−1922.

[28] Y.P. Zhu, T.Y. Ma, T.Z. Ren, J. Li, G.H. Du, Z.Y. Yuan, Appl. Catal. B: Environ. **157** (2014) 44− 52.

[29] S. Dehghanpour, A. Mahmoudi, F. Esbati, S.H. Rasanani, Mater. Res. Bull. **47(9)** (2012) 2126–2134.

[30] T.Z. Ren, X.H. Zhu, T.Y. Ma, Z.Y. Yuan, Ads. Sci. Technol. **31(6)** (2013) 535–548.

[31] M.A. Nistor, S.G. Muntean, B. Maranescu, A. Visa, Appl. Organomet. Chem. **34(11)** (2020) e5939.

[32] B. Maranescu, A. Visa, V. Maranescu, Phos. Sul. Sil. Rel. Elem. **190** (2015) 902–904.

[33] A. Farrokhi, F. Bivareh, S. Dejbakhshpour, A.Z. Moghaddam, Appl. Organomet. Chem. **34(11)** (2020) e5938.

[34] M. Pica, Molecules **26(8)** (2021) 2392.

[35] T.Y. Ma, X.Z. Lin, X.J. Zhang, Z.Y. Yuan, New J. Chem. **34** (2010) 1209−1216.

[36] P. Patel, U. Chudasama, U. Ion Exch. Lett. **4** (2011) 7−15.

[37] C. Duval, Inorganic Thermogravimetric Analysis, Elsevier, Amsterdam, 1963, p. 315.

[38] S. Patra, E. Roy, R. Madhuri, P. K. Sharma, J. Ind. Eng. Chem. **33** (2016) 226−238.

[39] S. Sultana, K. Islam, M.A. Hasan, H.J. Khan, M.A.R. Khan, A. Deb, M. Al Raihan, M.W. Rahman, Enviro. Nanotechno. Monitor. Manage. **17** (2022) 100651.

[40] M.S.U. Rehman, M. Munir, M. Ashfaq, N. Rashid, M.F. Nazar, M. Danish, J.-I. Han, Chem. Eng. J. **228** (2013) 228, 54–62.

[41] M.A.M. Salleh, D.K. Mahmoud, W.A.W.A. Karim, A. Idris, A. Desalination **280(1–3)** (2011) 1–13.

[42] K.Y.A. Lin, W.D. Lee, Appl. Surf. Sci. **361** (2016) 114-121.

[43] K.M. Elsherif, A. El-Hashani, I. Haider, J. Fund. Appl. Sci. **11(1)** (2019) 65-81.

[44] D. Son, B. Hai, V.Q. Mai, D.X. Du, N.H. Phong, D.Q. Khieu, J. Chemist. 2016, 1–11.

[45] Z. Chen, J. Fu, M. Wang, X. Wang, J. Zhang, Q. Xu, Appl. Surf. Sci. **289** (2014) 495–501.

[46] Y. Liu, Y. Huang, A. Xiao, H. Qiu, L. Liu, Nanomaterials **9** (2019) 51.

[47] M. Rahmani, M. Kaykhaii, M. Sasani, Spectrochi. Acta Part A: Mole. Biomole. Spectro. **188** (2018) 164-169.

[48] P. Saha, S. Chowdhury, S. Gupta, I. Kumar, Chem. Engg. J. **165(3)** (2010) 874-882.

[49] E.A. Abdelrahman, J. Mole. Liq. 253 (2018) 72-82.

[50] X. Peng, P. Yang, K. Dai, Y. Chen, X. Chen, W. Zhuang, H. Ying, J. Wu, Scient. Rep. **10 (1)** (2020) 9623.

[51] D.F. Romdhane, Y. Satlaoui, R. Nasraoui, A. Charef, R. Azouzi, J. Chem. **1** (2020) 1–17.

[52] H.L. Chieng, L.B.L. Lim, N. Priyantha, Desalin. Wat. Treat. **55** (2015) 664.

[53] P. Arabkhani, A. Asfaram, J. Hazard. Mater. **384** (2020) 121394.

[54] M. Mahramanlioğlu, S.I. Kirbasalar, I. Kizilcikli, Fresenius Environ. Bull. **12** (2003) 1483–149.

[55] X. Zhang, H. Yu, H. Yang, Y. Wan, H. Hu, Z. Zhai, J. Qin, J. Colloid Interface Sci. **437** (2015) 277-282.

[56] S.M. Ghonim, H.F. Youssef, M. Nassar, M.H. Shaltout, A.S. Amin, Egypt. J. Chem. **65(8)** (2022) 669-686.

[57] J. Wu, Q. Li, W. Li, Y. Li, G. Wang, A. Li, H. Li, J. Clean. Prod. **251** (2020) 119694.